Available online at www.sciencedirect.com
ScienceDirect
Progress in Particle and Nuclear Physics 60 (2008) 283–337
Progress in Particle and Nuclear Physics
www.elsevier.com/locate/ppnp

Review

From Ge(Li) detectors to gamma-ray tracking arrays – 50 years of gamma spectroscopy with germanium detectors

J. Eberth[a,*], J. Simpson[b]

[a] *Institut für Kernphysik, Universität zu Köln, D-50937 Köln, Germany*
[b] *STFC, Daresbury Laboratory, Daresbury, Warrington WA4 4AD, UK*

Abstract

The structure of the atomic nucleus has been studied to a large extent by gamma-ray spectroscopy using germanium (Ge) detectors. Ge detectors were developed in the 1960s and still offer the best compromise between energy resolution and efficiency for high-resolution gamma-ray spectroscopy. In the 1970s and 1980s the main advances were in the purity and volume of the Ge crystals. More recently the development of highly-segmented Ge detectors has significantly increased the performance and power of detection systems. In a segmented Ge detector the crystal is divided into sections by isolating the contacts. This enables the position of interaction to be determined. The accuracy of the position determination can be improved by the analysis of the shape of the charge signals and of the transient signals in adjacent segments. This technique has led to the concept of gamma-ray tracking in a segmented Ge detector whereby the energy, time and position of all interactions are recorded and the full interaction is reconstructed. This enables a spectrometer system with unprecedented efficiency and energy resolution to be realized. In this article, the history of Ge detectors and Ge detector arrays for nuclear spectroscopy will be reviewed. The technology and properties of highly-segmented coaxial Ge detectors as developed for the European γ-ray tracking array AGATA will be highlighted.

Keywords: Ge(Li) detectors; HPGe detectors; Escape suppressed spectrometers; 4π Ge γ-ray arrays; Ge γ-ray tracking arrays

* Corresponding author.
E-mail address: eberth@ikp.uni-koeln.de (J. Eberth).

0146-6410/$ - see front matter © 2007 Elsevier B.V. All rights reserved.
doi:10.1016/j.ppnp.2007.09.001

Contents

1. Introduction

The knowledge of the excitation modes of the atomic nucleus has been predominantly obtained during the last few decades by making use of the spectroscopy of γ rays depopulating the excited states. Gamma spectroscopy gives access to the most important observables of the excited nuclear states needed for the comparison with nuclear structure models. They include state excitation energy, the spin of the state from angular distribution or angular correlation, the parity from linear polarization, the magnetic moment from perturbed angular correlation measurements, the quadrupole moment from the reorientation effect and the transition probability from lifetime measurements. A vast variety of nuclear phenomena have been explored from these data, for example the variation of shell structures from stable to exotic nuclei, nuclear shapes and their coexistence and symmetries in the nuclear excitation modes. The nuclear levels of interest have been excited using a variety of reaction techniques. They include, Coulomb excitation of collective low-spin states, heavy-ion induced fusion–evaporation reactions, deep inelastic reactions, transfer reactions and fragmentation reactions. These result in excitation modes that emit gamma radiation over a wide range of energy (50 keV–10 MeV), a wide range of velocity (from at rest to up to 50% of the speed of light) and a wide range of multiplicity (up to $\approx$30). These modes all have different experimental challenges for the design of an efficient high-resolution detector system. The detector system needs to have good energy resolution, good peak-to-background ratio, high efficiency and good timing properties in order to extract the interesting

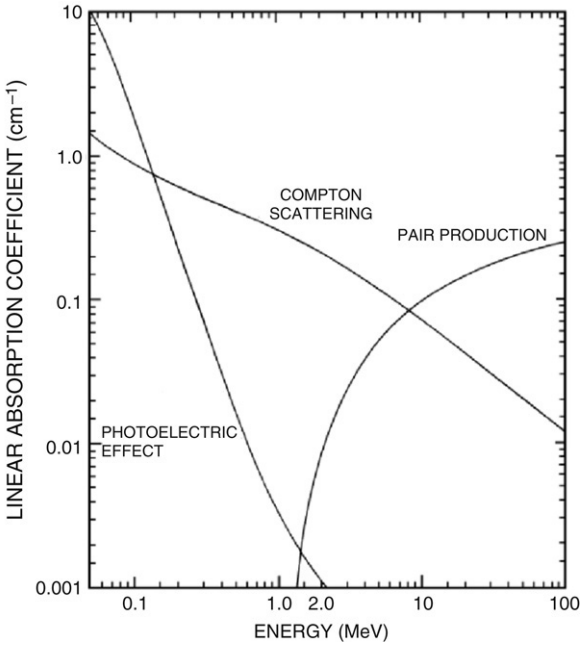

Fig. 1. Attenuation coefficients of γ rays interacting with germanium as a function of the γ-ray energy.

cascades of mostly rare events from these complex γ spectra. This article will focus on the properties of an optimum detector array which almost universally allows γ-ray spectroscopy to be performed in all these experimental conditions.

The design of the detector system needs to take into account the interaction processes that a γ ray undergoes as it interacts with matter. The three main processes are photoelectric absorption, Compton scattering and pair production. For γ energies ranging from a few 100 keV to a few MeV the Compton-scattering process is the most probable (see Fig. 1). If after single and multiple Compton scattering, part of the incident γ energy escapes from the detector, the event will contribute to the background of the spectrum. While the cross-section for the Compton effect varies linearly with Z of the detector material $\sigma_c \sim Z$, the cross-section for photo effect varies as $\sigma_{\text{photo}} \sim Z^{4-5}$ and for pair production as $\sigma_{\text{pair}} \sim Z^2$. Therefore, a high ordinal number Z of the detector material will increase the efficiency of the detector and reduce the background due to Compton scattering. In addition, the probability of full-energy absorption will increase with the volume of the detector and its density.

Does an ideal material for a γ-ray detector exist? Unfortunately the answer is no and a compromise between efficiency and resolution has to be sought. Crystal spectrometers [1] have a superb energy resolution of $\sim 10^{-5}$ but an extremely low efficiency. Gas detectors have a poor energy resolution and a too low density. Scintillation detectors like NaI(Tl), BGO or $LaBr_3$:Ce can have large volumes and high Z but their resolution is limited to a few percent. Semiconductor materials have some interesting properties that are beneficial for γ-ray detection. The energy needed to create an electron–hole pair is just a few eV, which yields a good energy resolution, and they can have a high Z. Semiconductors that have been used so far include Si, Ge, GaAs, CdTe, CdZnTe and HgI_2. Si has a low Z of $Z = 14$ and is very well-suited for the spectroscopy of X-rays and charged particles but γ lines corresponding to a few hundred keV will disappear

in the background of Compton-scattered events in a γ spectrum. GaAs, CdTe, CdZnTe and HgI_2 have a medium to high Z, which promises a good peak-to-total ratio in the γ spectra. In addition, the bandgap is large enough to operate the detectors at room temperature with low leakage current. Unfortunately, only rather small single crystals of some cm^3 have been grown so far. They also have much smaller charge carrier lifetimes as compared with Ge and they suffer from poor charge collection which degrades the energy resolution. Nevertheless, in the field of medical imaging these materials are gaining more and more importance. This is the case since in medical imaging the γ rays are mostly low in energy (100–500 keV) and the density of the lines in a spectrum is rather low so that the energy resolution is adequate for analysis. In addition, operation at room temperature makes their handling easier and safe, which is a big advantage for medical application. Significant progress has been achieved recently with the development of segmented or pixellized CdTe, CdZnTe and HgI_2 detectors. For the application discussed in this review, namely γ-ray spectroscopy in the energy range of 50 keV to 10 MeV, these materials are not well-suited because of the limited efficiency due to the small crystal size and the energy resolution, which is about a factor of three worse than that of a Ge detector.

The conclusion is that the best choice of material for universal in-beam γ-ray spectroscopy is still germanium. Ge has a bandgap of 0.7 eV, which results in a large number of electron–hole pairs being created, which in turn leads to small statistical fluctuations and hence good energy resolution. Typical line widths (FWHM) are $\Delta E_\gamma = 0.9$ keV at $E_\gamma = 60$ keV and $\Delta E_\gamma = 2$ keV at $E_\gamma = 1.3$ MeV. Rather large hyper-pure Ge crystals of up to 100 mm diameter and 140 mm length can now be grown routinely, which enhances the probability of total absorption of a γ quantum after multiple scattering in the crystal. Nevertheless, the choice of Ge is still a compromise. The consequence of the low atomic number of Ge of $Z = 32$ is that the Compton effect is the dominating interaction process for $E_\gamma > 180$ keV and even for the largest crystals only $\sim$25% of the events will contribute to the full-absorption peak and 75% will be background events in the Compton continuum in a γ-ray spectrum. Furthermore, the small bandgap of Ge favours the thermal excitation of electrons across the forbidden zone. This process can only be sufficiently suppressed by cooling the Ge detector in a vacuum cryostat to a temperature < 110 K. Liquid nitrogen is normally used for cooling and to a lesser extent mechanical cooling e.g. Stirling coolers. In both cases the cooling complicates the use of Ge detectors and in some cases limits their application. Table 1 summarizes the characteristics of different detector materials and Table 2 compiles in more detail the properties of germanium.

2. History and properties of the Ge detector

A Ge detector is not just a simple cooled pure crystal with two electrodes and a voltage to collect the charge carriers created by the incident radiation. In the crystal itself there is always a certain amount of impurities of valence 3 or 5 elements, which act as donors or acceptors in the Ge crystal (Ge is of valence 4). These donor or acceptor impurities have energy states that lie in the forbidden bandgap of the Ge crystal, close to the conduction and valence band, respectively. Therefore they are easily excited thermally, even at 77 K, to the conduction or valence band reducing the resistivity of the Ge crystal. Consider an example: the energy needed to create one electron–hole pair in Ge is $W = 2.9$ eV. A γ ray of 1 MeV, which is fully absorbed in the crystal, creates $\sim 3.5 \times 10^5$ electron–hole pairs. The number of free charge carriers in the crystal has to be much lower than this if the radiation-induced charge is to be collected with high accuracy, i.e. the number of donors and acceptors has to be in the order of 1000. Such an impurity concentration is at least 6–7 orders of magnitude below what is technically feasible. The solution is to build a

Table 1
Properties of some detector materials

Parameter	GaAs	Ge	$TeCd_{0.7}Zn_{0.3}$	CdTe	HgI_2
Density (g/cm^3)	5.32	5.33	5.5	5.85	6.4
Average atomic number	31.5	32	38	50	62
Bandgap (eV)	1.43	0.665	2.0	1.44	2.15
Pair creation energy (eV)	4.2	2.96	6.0	4.43	4.2
Electron mobility (cm^2/V s)	8000	3900	–	1100	100
Hole mobility (cm^2/V s)	400	1900	10	100	4
Electron lifetime (s)	10^{-8}	$> 10^{-3}$	–	3×10^{-6}	3×10^{-6}
Hole lifetime (s)	10^{-7}	2×10^{-3}	10^{-7}	2×10^{-6}	1×10^{-5}
Electron $\mu\tau$ product (cm^2 V^{-1})	8×10^{-5}	>1	$\sim10^{-4}$	3×10^{-3}	3×10^{-4}
Hole $\mu\tau$ product (cm^2 V^{-1})	4×10^{-6}	>1	10^{-6}	2×10^{-4}	4×10^{-5}
Crystal structure	Cubic (ZB)	Cubic	Hexagonal	Cubic (ZB)	Tetragonal
Lattice constant (Å)	5.6533	5.64613	–	6.48	4.37 (a) 12.44 (c)
Knoop hardness (kg mm^{-2})	750	692	–	60	<10
Melting point (°C)	1238	958	1320	1092	259
Dielectric constant	12.8	16	–	10.9	8.8
Resistivity (Ω cm)	10^7	50	10^{10}	10^9	10^{13}
$1/e$ abs. depth (mm) at 10 keV	0.051	0.050	0.019	0.011	0.011
at 100 keV	3.46	3.51	1.5	1.01	0.46
Typ. FWHM ΔE (keV) at 60 keV	0.7	0.3	1.8	1.1	3.5
Intrinsic FWHM ΔE (keV) at 60 keV (Fano noise)	0.439	0.250	0.530	0.300	0.409
Typical thickness (mm)	0.2	20	0.1	2	10

Table 2
Properties of germanium

Atomic number	32
Atomic weight	72.60
Stable isotope mass numbers	70–72–73–74–76
Density (300 K); g/cm^3	5.33
Atoms/cm^3	4.41×10^{22}
Dielectric constant (relative to vacuum)	16
Forbidden energy gap (300 K); eV	0.665
Forbidden energy gap (0 K); eV	0.746
Intrinsic carrier density (300 K); cm^{-3}	2.4×10^{13}
Intrinsic resistivity (300 K); Ω cm	50
Electron mobility (300 K); cm^2/V s	3900
Hole mobility (300 K); cm^2/V s	1900
Electron mobility (77 K); cm^2/V s	3.6×10^4
Hole mobility (77 K); cm^2/V s	4.2×10^4
Energy per electron–hole pair (77 K); eV	2.96
Fano factor (77 K)	<0.11

diode by doping n-type material (excess of donors) with acceptors or vice versa and to operate this diode in reverse-biased mode. This creates a so-called depletion layer in which almost no free charge carriers exist. This depletion layer will form the active volume for the detection of γ rays. Its thickness d is a function of the bias voltage U_b and the specific resistivity ρ of the Ge

material:

$$d \approx \sqrt{U_b \rho}. \tag{1}$$

The specific resistivity of a Ge crystal is given by the doping concentration, for n-type Ge, $\rho \sim 1/N_D$ where N_D is the donor concentration. In order to achieve a thickness of the depletion layer of a few cm at a bias voltage of $U_b = 5000$ V, a donor concentration of $<10^{10}$ cm^{-3} is needed. Such a low impurity concentration is at the limit of the technical feasibility and there are only a few facilities worldwide capable of growing Ge crystals of such a purity.

2.1. The Ge(Li) detector

The first Ge detectors produced had very small active volumes. The reason was that the impurity concentration of the purest Ge crystals that could be grown was too high to achieve even a mm thickness of the depletion layer (see Eq. (1)). However, in 1960 a very interesting process was developed, namely the compensation of the naturally occurring p-type excess impurities in Ge by introducing Lithium (Li) [2,3]. Li has valence 1 and acts as a donor on interstitial sites in the Ge lattice. The donor energy state lies in the forbidden gap of Ge just below the conduction band. At room temperature most of the valence electrons of Li are excited to the conduction band, i.e. the Lithium atom is ionised. Li is a very small atom, which has a high mobility in the lattice of Ge. A Ge crystal can be doped with Li by diffusion, which results in an exponential concentration profile of the Li with diffusion depth. If Li is evaporated onto the surface of an n-type Ge crystal and diffused for 10 min at ∼400 °C it will form an n^+-contact near the surface with an np transition in a depth of ∼1 mm. If this Ge diode is now reverse biased – at a temperature of 40–50 °C – the Li ions start to drift in the electric field of the diode to the cathode and compensate the acceptor concentration. It is a self-regulated process of the diode, which results in an almost perfect compensation of donors and acceptors. After a drifting time of weeks or months a thickness of the compensated layer of up to 35 mm can be achieved for a coaxial detector. The compensated layer has a high resistivity and is almost empty of free charge carriers. Application of a reverse bias results in a fully depleted layer [4]. The Li-drifted Ge detector has not only to be operated but also stored at low temperature. At room temperature the diffusion of Li would destroy, in a timescale of hours, the compensation profile.

The Ge(Li) detector sparked tremendous progress in nuclear structure physics from the late 1960s to ∼1980 and their development marked the birth of high-resolution γ spectroscopy. At the same time numerous accelerators for light and heavy ions were built and high-resolution in-beam γ-ray coincidence spectroscopy became possible for the first time. In parallel to the development of Ge(Li) detectors rather complex detectors with segmentation and composite Ge detectors, which were used as Compton polarimeters, were also developed [5–7].

2.2. The high-purity Ge detector

In the late 1970s high-purity Ge (HPGe) detectors became available commercially. Based on the pioneering research and development of the Berkeley group [8,9] n-type and p-type Ge crystals with a net impurity concentration of 5×10^9 to 2×10^{10} cm^{-3} could be grown. At this impurity concentration a maximum bias voltage of <5000 V is sufficient to deplete the full volume of a large coaxial diode. The HPGe detector has many advantages over the Ge(Li) detector. The production process of a detector is much faster since no time-consuming drifting process is needed. The HPGe detector still has to be operated at $T < 110$ K, but it can be stored at

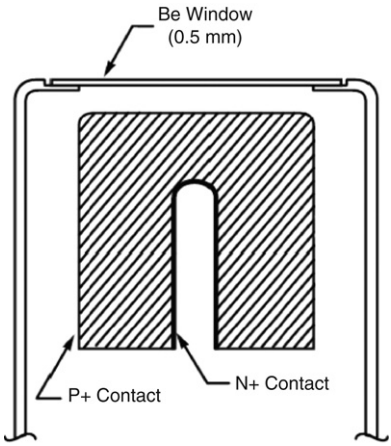

Fig. 2. n-type HPGe detector.

room temperature, which reduces storage cost and facilitates easier transportation. While Ge(Li) detectors have to be produced from p-type crystals, the HPGe detector can be made from p-type and n-type materials. HPGe n-type detectors (see Fig. 2) are less sensitive to neutron-induced radiation damage (see next chapter), which is a big advantage for their application in in-beam γ spectroscopy. The commercial production of Ge(Li) detectors was given up around 1980 when the volume of HPGe detectors became competitive with the volume of Ge(Li) detectors.

2.2.1. *Properties of the HPGe detector*

An HPGe detector is a diode produced from an extremely pure Ge single crystal. p-type as well as n-type crystals are used with a net impurity concentration of $\sim 10^{10}$ atoms cm^{-3}. The contacts of the diode are made by boron implantation on one side and by Lithium diffusion on the other side for both types of material. In p-type bulk material the Li-diffused contact forms the pn-junction and the boron-implanted contact limits the possible depletion layer, while for n-type material the contacts act in the opposite way. Fig. 3 shows the most common shapes of Ge detectors.

From the Poisson equation $\Delta\varphi = -\rho/\varepsilon$, where φ is the potential at any point, ρ is the charge density and ε the dielectric constant of the Ge crystal, the thickness d of the depletion layer as a function of the bias voltage V can be calculated. For a planar geometry d is

$$d = \sqrt{\frac{2 \cdot \varepsilon \cdot V}{\mathrm{e} \cdot N}} \tag{2}$$

with $\varepsilon = 16$, the dielectric constant of Ge, N, the dopant concentration
and for a true coaxial shape of the detector the depletion voltage V_d is given by

$$V_d = \frac{1}{2\varepsilon \mathrm{e} N}\left[r_1^2 \ln\left(\frac{r_2}{r_1}\right) - \frac{1}{2}(r_2^2 - r_1^2)\right] \tag{3}$$

with r_1 radius of the inner hole and r_2 radius of the crystal.

In practise, the thickness d of the depletion layer is limited in planar detectors to $\sim$2 cm. A larger detector volume can be achieved using a coaxial shape. From (3) it can be calculated that the depletion layer of a coaxial detector with a diameter of 90 mm can be extended over the

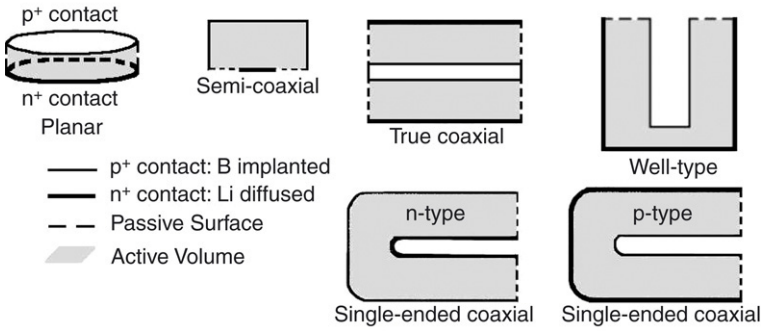

Fig. 3. Most common shapes of HPGe detectors.

whole volume of the crystal at a bias voltage of 5000 V and $N < 10^{10}$ 1/cm^3. Therefore, the planar detectors with their smaller volume but very uniform distribution of the electric field are preferred for the spectroscopy of low-energy γ rays in the range of 10 keV to a few hundred keV while coaxial detectors are used in the full-energy range of 10 keV to 10 MeV. The basic properties of HPGe detectors are well-described in textbooks [10,11] and shall not be repeated here. The aim of this review is to point out those technical and physical details which governed the development of the detector arrays for in-beam γ-ray spectroscopy during the last twenty five years and to discuss the limitations given by the present detector technology and to discuss future perspectives. Among the detector shapes shown in Fig. 3 the coaxial Ge detector with one closed end is chosen as the basis for almost all existing and planned γ-ray arrays in nuclear science research. Therefore, this review will concentrate the discussion on this type of detector.

The detector shape: true coaxial vs. closed-end coaxial detectors. It is obvious that the electric field in a closed-end coaxial detector is less uniform than in a true coaxial detector. Charge collection at the corners of the closed end is slower due to the weaker field and the longer collection path. The consequences are a poorer time resolution of the closed-end detector compared with a true coaxial detector and poorer energy resolution since the number of trapping centres along the longer path to the corners is appreciable. Why are then true coaxial detectors not used in modern day spectrometers? The answer lies in the properties of the intrinsic surface of the detector at the open end. This surface is the most critical part of any Ge detector as the full bias voltage is applied across the surface. The intrinsic surface has to be electrically passive and of high resistivity in order to avoid surface leakage currents. In Si detectors this is achieved by oxidation of the surface. In contrast to SiO_2, Ge oxides are chemically not very stable as they are water soluble. Therefore, the intrinsic Ge surface has to be protected by an isolating layer which consists for example of a sputtered layer of SiO_2 or a sputtered layer of amorphous Ge. These so-called passivation layers can cause additional problems. Active surface charges can bend the electric field in the detector away from the surface. The consequence is surface channels of very low-field strength where charges cannot be collected [12]. These dead layers at the intrinsic surface of a coaxial Ge detector have been measured to extend from 1 to 2 mm at the outer radius to 5–7 mm at the inner contact of the detector. The result of such a measurement is shown in Figs. 4 and 5. A single-ended n-type HPGe detector of 70 mm diameter and 78 mm length was mounted in a cryostat with its passivated intrinsic surface pointing to the entrance window of the cryostat and scanned with a collimated ^{241}Am source [13]. Examples of the measured spectra are given in Fig. 4. The strong attenuation of the 59.5 keV ^{241}Am transition by the passivated

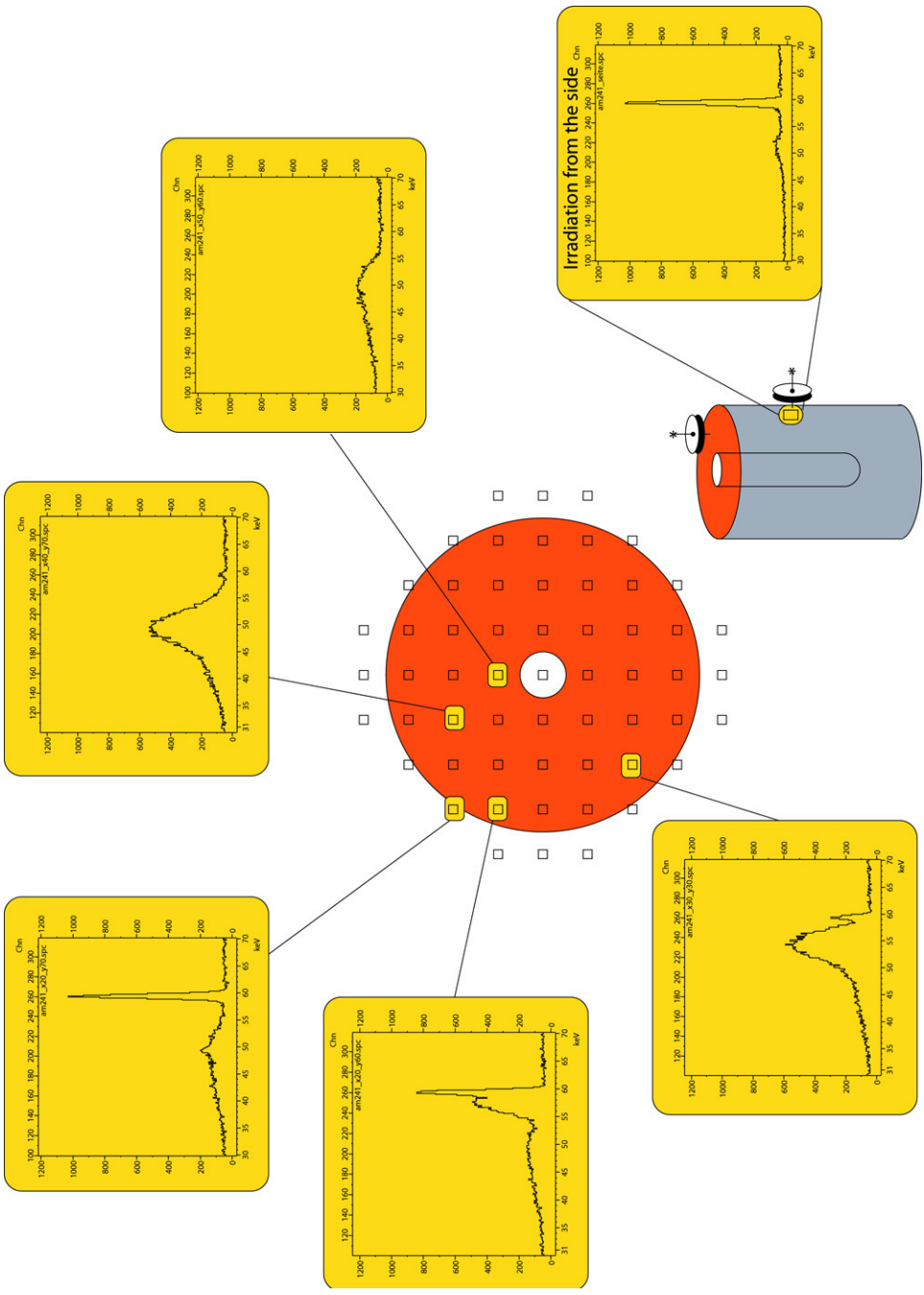

Fig. 4. Scan of the passivated intrinsic surface of an n-type HPGe detector with a collimated ^{241}Am source.

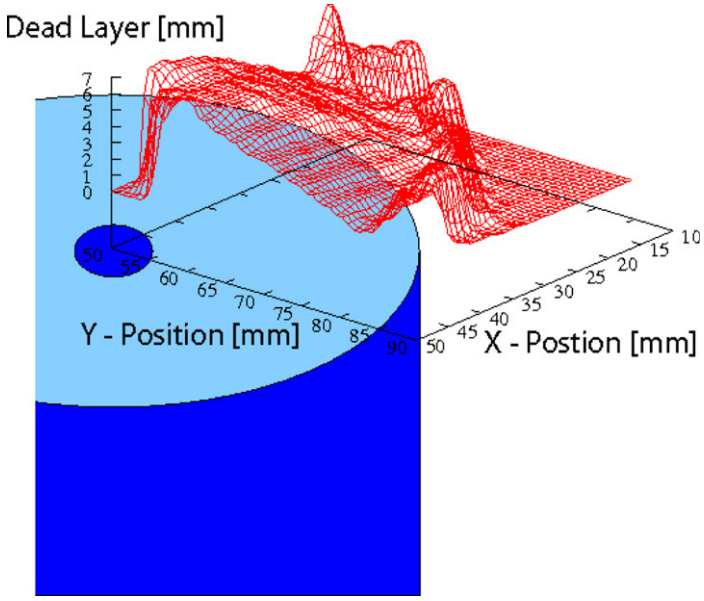

Fig. 5. Measured thickness of the dead layer caused by passivation of the intrinsic surface of an n-type HPGe detector.

detector surface is obvious. Only when irradiating the detector close to the outer diameter of the crystal or through the side surface can the ^{241}Am transition be measured with a good peak-to-total ratio. The thickness of the dead layer calculated from the attenuation of the ^{241}Am line is shown in Fig. 5 for one quarter of the intrinsic detector surface.

Successful passivation is not an easy process to achieve. Indeed, if a detector fails after production or during operation the failure is often due to non-perfect surface passivation. A true coaxial detector has these problems at the intrinsic surfaces at both ends of the crystal and the γ rays would have to enter the active volume through a dead layer of some mm thickness, which is not acceptable due to the absorption. However, the uniform electric field of a true coaxial detector would facilitate more simple pulse-shape analysis of position-sensitive detectors as is discussed later. Therefore, research is needed in order to find a better method of passivation.

n-*type vs* p-*type material.* The rectifying contact of a coaxial detector is usually placed at the outer surface of the crystal because this results in a lower field strength at the contacts when applying the depletion voltage. Thus, a p-type detector has a Li-diffused outer contact and an inner boron-implanted one while for an n-type detector the contacts are placed in the opposite way. Li-diffused contacts have typically a thickness of 0.6 mm while the boron-implanted contact is only 0.3 μ thick. Therefore, an n-type detector has a very thin entrance window for the radiation, which is an advantage especially for the spectroscopy of low-energy γ rays. Another reason, why n-type detectors are preferred to in-beam γ-ray spectroscopy is that these detectors are less sensitive to neutron-induced radiation damage. Fast neutrons are emitted in almost any nuclear reaction with projectile energies above the Coulomb barrier. These fast neutrons can impart enough energy to the Ge nuclei of the detector to dislocate the Ge atoms from their lattice position. The dislocations act as traps for holes which deteriorates the charge collection in the detector and hence the energy resolution. In an n-type detector the holes are collected at the outer p^+-contact while they have to travel to the inner core contact in a p-type detector. Most γ rays interact with the Ge detector close to the outer contact because most of the volume is

concentrated there. The hole traps are distributed uniformly throughout the crystal, therefore the holes will have a shorter average collection path in an n-type detector than a p-type detector. This results in a p-type Ge detector being an order of magnitude more sensitive to radiation damage introduced by fast neutrons than an n-type detector. For an n-type detector the influence on the energy resolution becomes visible after an integral flux of 2–4 10^9 n cm^{-2} [14–16].

Operating temperature of Ge detectors. A Ge detector has to be cooled in order to suppress the thermal excitation of electrons across the forbidden energy gap of 0.7 eV. At a reverse current of the Ge diode of <100 pA the noise contribution of thermal excitation starts to play a minor role which normally is already the case for a temperature of <120–130 K. Then neutron-induced radiation damage as a function of the operating temperature has to be considered. An investigation of this dependence on neutrons from fusion–evaporation reactions showed no effect below 120–130 K [17]. At higher temperatures the neutron-induced dislocations start to move forming clusters of dislocations with strongly enhanced trapping of holes. These clusters of traps can only be removed by annealing the detector. Therefore, a detector which has been exposed to some neutron flux should be kept cold (<130 K) or annealed. Statements on the optimal operation temperature of Ge detectors are somewhat contradictory in the literature. On the one hand, neutron-damaged detectors should be operated as cold as possible (<85 K) as thermally excited electrons reinforce the effect of hole trapping [20]. On the other hand, the Ge crystal may contain impurities which form shallow electron traps just below the conduction band. Already at temperatures of 85–90 K the trapped electrons can be thermally excited to the conduction band improving the energy resolution of the detector. From experience with some 150 EUROBALL detectors that have been operational for more than 10 years, it was found that these detectors should not be operated below 85 K and that a temperature of 85–95 K is the best compromise for the optimum energy resolution. The cryostats described later for the more recent projects, MINIBALL and AGATA, are therefore designed for the Ge detectors to be operated at 85–95 K.

Annealing of neutron-damaged Ge detectors. Hole traps due to neutron-induced lattice defects can be removed by annealing the Ge crystals for 1–3 h at 105 °C [21]. The detectors are normally heated in their cryostat via the cold finger while keeping the pressure of the cryostat at $\sim 10^{-6}$ mbar with a turbomolecular pump in order to avoid contamination of the intrinsic detector surface. Encapsulated Ge detectors as used for the EUROBALL cluster, MINIBALL, AGATA and GRETINA detectors (see Sections 4 and 5) can be easily removed from the cryostat and annealed by heating in a standard oven. This has the advantage that only the encapsulated detector itself is heated and not the cold components of the preamplifier, which might be damaged by the procedure. The annealing parameters given above refer to encapsulated detectors where the temperature of the crystal can be measured easily at the capsule surface. The standard (not encapsulated) coaxial Ge detectors that have to be annealed in the cryostat normally use dc coupled preamplifiers to read out the detector signal at the core electrode. In this case the outer contact of detector, the crystal holder and the heat shield are at the high potential of the bias voltage and have to be electrically isolated from the cold finger. The "crystal temperature" then is measured with a PT100 resistor at the cold finger and not at the crystal itself. The procedures for the annealing of standard detectors in the cryostat reported in the literature mostly recommend an annealing temperature of 100–120 °C and an annealing time of several days. The long annealing time compared with encapsulated detectors is suggested since the temperature of the crystal is considerably lower than that measured at the cold finger.

The n^+*- and* p^+*-contact of the Ge detector.* The Ge detector needs highly-doped contacts (indicated by the label "+"). One contact forms the pn-junction while the other highly-doped contact avoids charge injection when the detector is fully depleted. The commercially produced

n-type detectors so far use boron-implanted p^+-contacts and Li-diffused n^+-contacts. While the boron-implanted contact is very thin and gives only a dead layer of 0.3 μm, the Li-diffusion process results in a typical dead layer of 0.6 mm. Segmented contacts are the basis for position-sensitive Ge detectors as discussed in chapters 4 and 5. Boron-implanted contacts can be segmented by photolithographic methods [22]. Li-diffused contacts can only be segmented mechanically by cutting groves using either ultrasonic grit, a diamond saw or deep reactive ion etching. If these detectors are stored at room temperature or annealed from neutron damage the segment separation can be lost by Li-diffusion under the groves. Therefore, it would be better to replace the Li-diffused contact by another technology. A possibility is to implant an element of valence 5 like phosphorous. P-implantation has been studied in the past and some good results were reported [23]. However, the problem of P-implantation is the large lattice damage caused by the relatively big phosphorous atom during implantation. Subsequent annealing of the crystal helps, but does not remove the damage completely. The remaining lattice damage easily results in charge injection which affects the energy resolution of the detector. It has been shown recently [24,25] that contacts of both types can be produced by sputtering a layer of amorphous germanium onto the etched surfaces of the Ge crystal. The resulting contacts are thin and have a high resistivity. The active areas of the detector are defined by evaporated metal layers (e.g. Au or Al). Using masks during the evaporation process allows an easy segmentation of the detector. The first results are very encouraging. However, further research and development is needed before these detectors might become the commercial standard.

Charge collection and energy resolution. Gamma rays interact in Ge detectors by photo absorption, Compton scattering or production of electron–positron pairs (for details see e.g. [10]). The fast electrons and positrons created by these processes are stopped in the detector by electron scattering producing electron–hole pairs. In the electric field of the Ge diode the electrons move to the n^+-contact while the holes move to the p^+-contact. As the charge carriers move they induce a current on the contacts. The shape of the detector signal depends on the electric field strength, the drift velocity of the electrons and holes and the distance of the interaction from the contacts. The electric field itself depends on the spatial impurity distribution in the crystal. The impurity concentration can be measured only at the surface of the crystal and normally a linear radial as well as an axial gradient between the values measured at the surface is assumed. The theoretical description of the signal shape becomes important for the calibration of position-sensitive detectors. Therefore, this will be discussed further in Section 5 for the AGATA detectors.

The average energy for the creation of one electron–hole pair in Ge is 2.96 eV at 90 K although the bandgap of Ge is only 0.74 eV at 90 K. The energy difference is due to the excitation of lattice vibrations, a process with competes with the creation of electron–hole pairs. As these two processes are correlated, the Poisson statistics cannot be applied to calculate the variance of the number of created electron–hole pairs. A correction factor was introduced by Fano from theoretical considerations. As a quantitative calculation of the Fano factor F is still missing, F has been estimated from the best energy resolution measured with small Ge detectors to be $F \sim 0.1$. The contribution to the FWHM of a γ line by the statistical fluctuation is then given by

$$\Delta E_\gamma = 2.35\sqrt{F \cdot 2.96 \cdot E_\gamma} = 1.28\sqrt{E_\gamma}. \tag{4}$$

The other main contribution to the energy resolution comes from the detector current and the noise of the preamplifier. The bulk current of the cold Ge diode is typical of only a few pA and its contribution to the energy resolution can be almost neglected. The critical point is

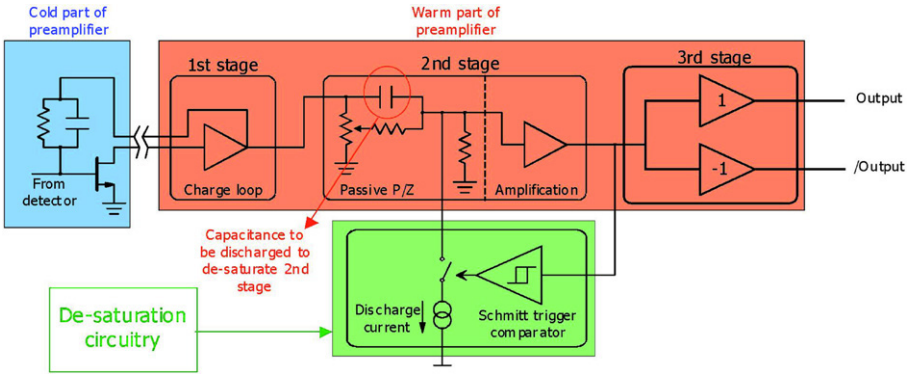

Fig. 6. A modern charge-sensitive preamplifier with differential output and a de-saturation stage for high count-rate capability as used in AGATA [18,19].

surface currents due to an imperfect passivation of the intrinsic surface or surface contamination. The noise contribution of the preamplifier and especially of the field-effect transistor (FET) at the input stage makes a significant contribution to the resolution. The charge generated by a γ interaction in the detector is rather small. Therefore, a high gain of the FET is used which also amplifies the noise of the input stage. Fig. 6 shows a schematic diagram of a charge-sensitive preamplifier with resistive feedback, typically used with Ge detectors [18,19]. The circuit includes a differentiation of normally 50 μs.

The noise of a charge-sensitive preamplifier grows proportional with the input capacitance [10], i.e. with the detector capacitance. For very low-preamplifier noise typical values are for feedback $R_F = 100$ GΩ and $C_F = 0.5$ pF. The resulting high gain of the preamplifier, however, then reduces the count-rate capability of the preamplifier which is limited by pile-up of the signals with their 50 μs fall time and the maximum output voltage. For high-count rates a typical feedback network is $R_F = 1$ GΩ and $C_F = 1.2$ pF. Modern preamplifiers of this type give a noise contribution of $\Delta E_{\text{preamp}} = 0.6\ \text{keV} + (10\ \text{eV/pF}) \cdot C_D$, where C_D is the capacitance of the detector. A large coaxial detector of 80% efficiency (see next section) has a capacitance of $C_D = 45$ pF. This value then gives a noise contribution of the preamplifier of $\Delta E_{\text{preamp}} = 1.05$ keV. The noise of the preamplifier and the statistical fluctuation of the charge carriers are statistically independent and have to be added quadratically. For an ideal detector (no surface currents, no charge losses) the estimated FWHM is

$$\text{at } 122\ \text{keV } (^{57}\text{Co}): \ (\Delta E_\gamma)^2 = (0.447)^2 + (1.05)^2 = 1.30, \quad \Delta E_\gamma = 1.14\ \text{keV}$$
$$\text{at } 1332.5\ \text{keV } (^{60}\text{Co}): (\Delta E_\gamma)^2 = (1.478)^2 + (1.05)^2 = 3.29, \quad \Delta E_\gamma = 1.81\ \text{keV}.$$

The energy resolution of a good detector is not far away from these values provided that a proper shaping of the signal in the main amplifier has been applied. In most main amplifiers the preamplifier output signal is formed by a network of RC differentiators and RC integrators to produce a Gaussian shape. This removes the signal pile-up of the preamplifier and limits the bandwidth to the frequency range corresponding to the rise time of the detector signal. Suppressing low and high frequencies not needed for the signal reduces noise and improves the energy resolution. Large shaping times lower the noise contribution of the FET while smaller shaping times reduce the noise contribution due to the leakage current of the detector (for details see [10]). A large coaxial detector with low leakage current will have the best energy resolution

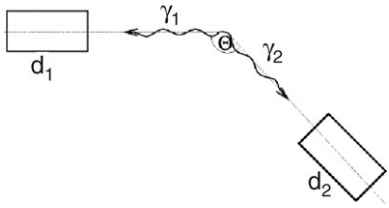

Fig. 7. Coincidence setup for the determination of the detector efficiency.

at rather long shaping times of $\tau_{\text{diff}} = \tau_{\text{int}} = 6$–$10$ μs. Because of pile-up the large signal width limits the count-rate capabilities. If higher count rates are needed the shaping time has to be reduced and a loss in energy resolution of a few hundred eV has to be accepted. Sometimes a detector has a poor energy resolution and the possibility of high leakage current has to be investigated. This can be easily checked because of the specific dependence of the current noise on shaping times. If the energy resolution improves when going to short shaping times of 2 or 1 μs, then it is clear that the leakage current is too high.

Efficiency. The intrinsic full-energy peak efficiency ε_p is defined as the ratio of the number of counts in the full-energy peak divided by the number of incident γ rays. The absolute full-energy peak efficiency ε_a at a given distance is defined as the ratio of the number of counts in the full-energy peak divided by the number of γ rays emitted by the source. The problem with these definitions is that it is not easy to calculate from the efficiency measured at one source to detector distance the efficiency at another distance as the measured intensity does not scale directly with $1/r^2$, where r is the distance from the source to the detector front face. The virtual point for $r = 0$, the point of interaction, lies at some energy dependent distance behind the front face. In addition, at close distances the γ rays see a different detector thickness from the centre of the detector to its corners. This effect also depends on the shape of the detector. To avoid these problems and since the NaI(Tl) detector was the standard for γ-ray spectroscopy in the 1960s a relative efficiency was defined when the first Ge detectors became available. This relative full-energy peak efficiency is defined as the ratio of the full-energy peak efficiency of the Ge detector for the 1332.5 keV ^{60}Co line at a distance of 25 cm between the source and the detector surface divided by the absolute efficiency of a $3'' \times 3''$ NaI(Tl) detector (1.2×10^{-3} [26]) at the same distance. The relative efficiency of a Ge detector can be determined from a ^{60}Co singles spectrum if the activity of the source is known. The error of the efficiency value then will be given normally by the error of the known activity, since sources with very accurate activity are seldom available. The other possibility is to measure the efficiency from a γ–γ coincidence technique. In this case the activity of the source does not need to be known. ^{60}Co emits two cascading photons of almost the same intensity, a crossover transition, if existing at all, can be neglected. The setup for this measurement would consist of two Ge detectors. Detector 1, for which the efficiency is to be measured, is placed at 25 cm distance from the source and another Ge detector is placed at an angle θ with respect to detector 1 (see Fig. 7). The efficiency of the second detector does not need to be known.

If N_1 is the number of counts detected for the 1173.2 keV transition in detector 1, N_2 the number of counts in the 1332.5 keV line measured in detector 2, N_{12} the number of coincidences, $\varepsilon_{a1,2}$ the absolute efficiency of the detector 1, 2 and A the activity of the source, then the following relations hold

$$N_1 = \varepsilon_{a1} A, \qquad N_2 = \varepsilon_{a2} A, \qquad N_{12} = \varepsilon_{a1}\varepsilon_{a2} A \cdot W(\theta) \tag{5}$$

where $W(\theta)$ is the angular correlation function and θ is the angle between the two γ rays. The three equations can be solved for the three unknown ε_{a1}, ε_{a2} and A:

$$\varepsilon_{a1} = \frac{N_{12}}{N_2 W(\theta)}, \qquad \varepsilon_{a2} = \frac{N_{12}}{N_1 W(\theta)}, \qquad A = \frac{N_1 N_2}{N_{12}} W(\theta). \tag{6}$$

From the first relation, the absolute efficiency of detector 1 has to be divided by 1.2×10^{-3} to determine the relative efficiency of the Ge detector 1. The third relation can be used for an accurate determination of the source activity which can be used for subsequent efficiency measurements using the γ-singles technique.

An elegant variation of the coincidence method is to extract the number of coincidences N_{12} from the sum peak in the singles spectrum. The ^{60}Co source is positioned at 25 cm distance from Ge surface of a detector of unknown efficiency and a singles spectrum with good statistics is collected. N_1 is again the number of counts in the 1173.2 keV line and N_2 the number of counts in 1332.5 keV line. Then, coincidences between the two transitions, which interact within the short lifetime of the intermediate ^{60}Ni level with the detector, will be added and appear in the spectrum as sum peak with an energy of 2505.7 keV. The number of counts in the sum peak is N_{12} and the above formulas can be used without modification. In this case the angle θ is $\theta = 0°$ and the angular correlation function for the ^{60}Co cascade has the value $W(\theta = 0) = 1.074$. A correction for the solid angle of the detector can be neglected at a source–detector distance of 25 cm. The sum peak intensity can also be corrected for random coincidences. These random coincidences occur when γ rays from the decay of two different ^{60}Co nuclei are added. Besides giving a contribution to the sum peak at 2505.7 keV, the combinations 1173.2 keV + 1173.2 keV = 2346.4 keV and 1332.5 keV + 1332.5 keV = 2665 keV will be added randomly and appear as additional small peaks in the spectrum. The intensity I_γ of the random coincidences to be deduced from the sum peak of true coincidences is then given by:

$$I_r\ (2505.7\ \text{keV}) = (I_r\ (2364.4\ \text{keV}) + I_r\ (2665\ \text{keV}))/2.$$

At small distances between the ^{60}Co source and the Ge detector the intensities measured for the 1173.2 and 1332.5 keV transition have to be corrected for intensity losses due to the summing effect. At a distance of 25 cm this loss is in the order of 10^{-3} and it can be neglected for the determination of the relative efficiency.

3. Gamma-ray detector arrays

As soon as Ge(Li) detectors of a few % relative efficiency became available they were used in coincidence experiments studying nuclei populated in the decay of long-lived isotopes as well as nuclei populated by fusion–evaporation reactions at particle accelerators. For the first time, the efficiency and the energy resolution of a detector was good enough to filter cascades of γ rays out of the complex in-beam spectra and to establish detailed level schemes up to a spin I = 16–20 [27]. An example of the new physics was the discovery of backbending, the alignment of pairs of particles in time-reversed orbits, by Johnson et al. in 1971 [28]. This was identified in a γ–γ coincidence experiment with two small Ge(Li) detectors. The fast progress of nuclear structure physics in the early 1970s was clearly related to the advent of the Ge(Li) detector. It was now possible to determine spins of excited states from the angular distribution or correlation of γ rays and the parity from the measurement of the linear polarization of the γ rays. The lifetime of excited states could be measured with the Doppler Shift Attenuation

Method (DSAM) or the Recoil Distance Method (RDM), in both cases using Ge(Li) detectors. It was amazing how many different nuclei were studied in the late 1960s and the early 1970s for the first time. However, these new experimental techniques soon reached their limits. After studying the energetically low lying fundamental excitation modes of nuclei in or close to the valley of stability the natural goal became to extend the investigations to rare excitation modes, higher spins, higher excitation energies and to nuclei with more exotic neutron-to-proton ratios, and consequently the desire to study weaker and weaker γ-ray intensities. Unfortunately, the identification of weak γ rays was strongly limited by the peak-to-background ratio of the spectra measured with small Ge detectors. The cross-section for Compton scattering dominates in Ge for $E_\gamma > 180$ keV and the probability that the Compton-scattered γ rays escape from a small Ge detector is high. Therefore, the peak-to-Compton ratio of the first Ge detectors was poor, with more than 90% of the interactions contributing to the Compton distribution and only less than 10% to the full-energy peak. The Compton continua of all the γ rays summed and made it difficult to detect a weak full-energy peak on the Compton background created by the strong γ rays.

How could the background be reduced? One improvement came gradually as the crystal pullers learned to grow larger and larger detector-grade Ge crystals. The peak-to-Compton ratio increases with the volume of the detector as multiple Compton scattering and photo absorption of the scattered low-energy γ rays become more likely. In addition, the growing size and efficiency of the detectors increased the coincidence rate and improved the statistics. For almost 10 years between 1970 and 1980 a standard setup for γ-ray spectroscopy consisted of two or a few Ge(Li) detectors.

The next major step in the development was the introduction of escape-suppression shields. The Ge detector was surrounded by a NaI(Tl) scintillator, which had only two holes, one to insert the Ge detector and one to provide the entrance for the γ rays [29,30]. The majority of the γ rays that are scattered out of the Ge detector were then detected in the NaI(Tl) scintillator. This was used to produce a veto signal that rejected the partly absorbed events from the spectra of the Ge detector. The reduction of the Compton background was to a factor of 10 using such an escape-suppression shield and for γ-singles measurements this was a big improvement. In coincidence spectroscopy with two such systems the improvement was not so clear since the Ge's were located much further from the radiation source. Improved spectrum quality was offset by a loss in coincidence efficiency. The solution to this issue was to increase the number of escape-suppressed Ge detectors.

3.1. The first γ-ray array TESSA: NaI(Tl) suppression shields and Ge(Li) detectors

The first array of escape-suppressed Ge detectors for in-beam experiments was built in 1980 in Risø, Denmark by a collaboration of the Niels Bohr Institute and the University of Liverpool. The array, called TESSA (the Escape Suppressed Spectrometer Array), consisted of 5 Ge(Li) detectors of ∼25% relative efficiency each and NaI(Tl) escape-suppression shields [31–33]. The escape-suppression shields were NaI(Tl) cylinders of 25 cm diameter and 20 cm length which filled almost the complete solid angle around the target as shown in Fig. 8. Collimators protected the shields from the direct radiation from the target. An excellent peak-to-total ratio of ∼60% could be achieved with these NaI(Tl) shields, but their sizes limited the number Ge detectors that could be placed around the target to 5–6. This array led to a revolution in γ-ray spectroscopy with a plethora of new nuclear structure phenomena being observed [33].

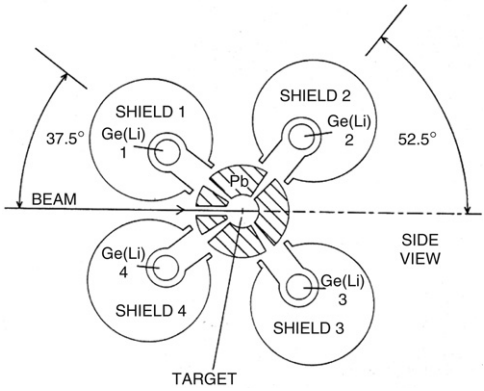

Fig. 8. The TESSA spectrometer comprising Ge detectors with NaI(Tl) escape-suppression shields.

3.2. HERA: BGO suppression shields and n-type HPGe detectors

The first TESSA spectrometer had a considerable impact on the development of further arrays. The direction was escape-suppression shields for background reduction and as many Ge detectors as possible in order to achieve good statistics for coincidence spectroscopy. The next remarkable step in the development was the HERA spectrometer (high-energy resolution array) which was built at the beginning of the 1980s at the Lawrence Berkeley National Laboratory [35,36]. HERA made use of two innovations, the BGO ($Bi_4Ge_3O_{12}$) scintillator and the n-type HPGe detector. Bismuth germanate has a higher average Z and a higher density than NaI(Tl). It is about three times more efficient per interaction length than NaI(Tl). This feature allowed a considerable reduction of the size of the suppression shields and thus gave space for more Ge detectors. A disadvantage of BGO is the lower light output as compared with NaI(Tl). Therefore, many of the suppression shields described in the next chapters (including HERA) used NaI(Tl) around the entrance opening for the γ rays in addition to the main BGO shield to improve the efficiency for the detection of the low-energy γ rays that are backscattered from the Ge detector. The other innovation was the use of n-type HPGe detectors which just had become commercially available. Coaxial n-type Ge detectors have a thin boron-implanted p^+-contact at the cylinder surface, which is well-suited for combination with an escape-suppression shields as there is less dead material between the Ge detector and the scintillator. HERA consisted of 21 HPGe detectors of $\sim$25% efficiency arranged in three rings around the target, see Fig. 9. The BGO detectors have a diameter of 13 cm and a length of 12.5 cm. They are tapered at the front part to 20° to enable a closer distance of the Ge detector to the target. A peak-to-total ratio of 50% was achieved with these BGO shields. The free space around the target was filled with an inner ball of 44 BGO detectors arranged in three concentric rings and with holes in front of the Ge detectors. The purpose of the inner ball was the measurement of the multiplicity and the total energy of the emitted γ rays.

The big impact made by HERA was that the total efficiency at 1.3 MeV of the Ge detectors (1.5%) made it possible for the first time to measure sufficient γ–γ–γ coincidences in a few days of beam-time. Double gating on a γ-ray cascade of interest reduces the background to other reaction channels, as is discussed later in more detail. A further background reduction was achieved by gating on the γ multiplicity and on the total energy measured with the inner ball.

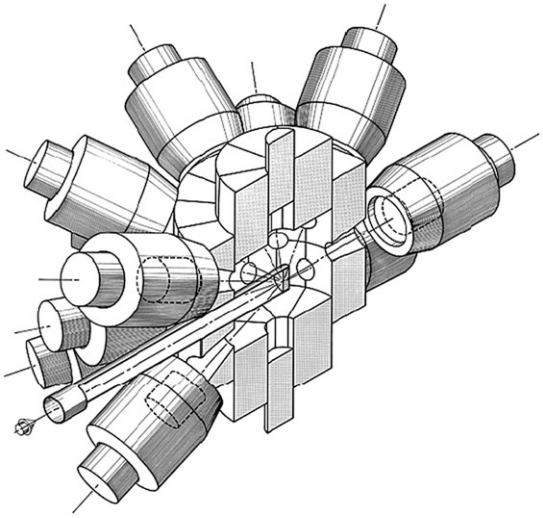

Fig. 9. The γ-ray array HERA.

3.3. Other arrays of the 1980s

A number of other arrays were built in the 1980s, all using BGO suppression shields and 12–30 n-type Ge detectors of 25%–35% relative efficiency. The cost of these arrays was still in the range of national funding and allowed a fruitful competition and enabled complimentary experiments to be performed at a range of different accelerator laboratories in nuclear structure physics. All these arrays looked somewhat different, had some specific improvement in technology and were adapted to the specific scientific interest of the collaborations.

The TESSA arrays: The TESSA arrays were continuously improved and upgraded at Daresbury Laboratory in the UK [32,33]. TESSA3 which became well-known for the discovery of super-deformation in ^{152}Dy [41] consisted of 16 Ge detectors with BGO shields. The European collaboration array ESSA30 with 30 detectors was also operated at Daresbury Laboratory. A version of the TESSA spectrometer was coupled to the Daresbury recoil mass separator [34] for identification of the reaction channel.

OSIRIS: This array was built by a German collaboration and was used at the cyclotron VICKSI at Berlin and at the Cologne FN tandem accelerator. It comprised 12 HPGe detectors of 25%–35% efficiency. Six detectors were shielded by cylindrical BGO detectors and 6 by asymmetric shields where the Ge detector was inserted perpendicular to the γ-ray flux [37]. A "golf club" cryostat allowed the entrance hole of the Ge detector to be closed by a NaI(Tl) plug for optimal escape suppression. OSIRIS had an inner BGO ball and an array of neutron detectors at forward angles with respect to beam axis for the investigation of proton-rich nuclei by neutron$-\gamma-\gamma$ coincidences.

The Argonne National Laboratory used an array of 12 "golf club" detectors with asymmetric BGO shields.

Nordball. This array was built by a Scandinavian collaboration and operated at Risø, Denmark. It used 20 BGO shielded Ge detector telescopes [38]. In each cryostat a planar Ge detector was mounted in front the coaxial detector. High energy γ rays passed through the planar detector and interacted in the coaxial detector. Low-energy γ rays interacted most likely with the planar

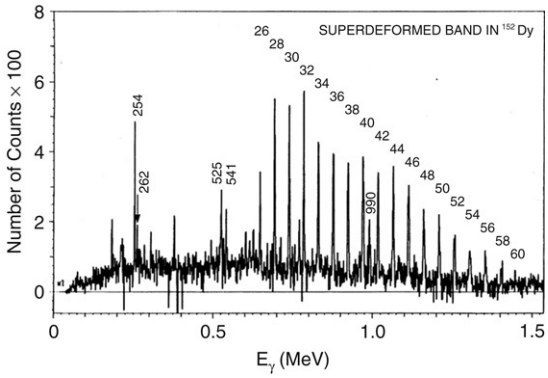

Fig. 10. Coincidence spectrum of the super-deformed band in ^{152}Dy [41].

detector. The condition that there was no coincident event in the coaxial detector meant that fully absorbed events in the planar detector were enhanced and the background at low energies strongly suppressed. The other speciality of Nordball was an inner shell of 60 BaF_2 detectors with holes to allow radiation to pass directly to the Ge detectors. The fast timing of the BaF_2 detectors (300 ps) allowed neutron events to be separated from γ events by time-of-flight in addition to acting as a γ multiplicity and sum-energy device.

Chateau de Cristal. This array was built by a French collaboration and operated at Strasbourg [39]. It consisted of 12 escape suppressed systems. BaF_2 was used for the composite escape suppressors as well as for the inner ball of 38 scintillators. All 72 BaF_2 elements together could be used as a γ-ray spectrometer with excellent timing properties.

8π Spectrometer. This array was developed at Chalk River, Canada and used 20 BGO shielded Ge detectors in a spherical arrangement [40]. The inner BGO ball had a very regular shape and consisted of 72 detectors, 60 of which had a hexagonal shape and 12 a pentagonal shape. By this design the multiplicity resolution was optimized, but the distance of the Ge detectors from the target had to be rather large (27 cm) reducing the absolute efficiency of the Ge detectors.

In summary, different technical advances and specific designs for γ-ray arrays were exploited in 1980s and resulted in a wealth of successful nuclear structure experiments. The experimental experience with these different spectrometers provided the basis for the next big step in the development of γ-ray arrays which will be described in Section 3.5.

3.4. Impact on nuclear structure physics

The experimental progress of the new arrays was based on the possibility to measure γ–γ–γ coincidences. Double gating and ancillary detectors allowed to isolate weak cascades of γ rays and to follow the γ-ray flux from the ground state up to spin 50–60$\hbar$. Among the many discoveries based on these improved experimental techniques the most striking one was the discovery of super-deformed (SD) states at high spins in nuclei. Fig. 10 shows a spectrum of the classic SD-band in ^{152}Dy [41]. The regular pattern of narrow-spaced γ lines was interpreted as resulting from the rotation of an axially deformed nucleus with a major-to-minor axis ratio of 2:1. This large deformation was confirmed by the measurement of the transitional quadrupole moment of the band [42]. Many other examples of SD-bands were soon found in other nuclei which allowed a systematic experimental and theoretical investigation. SD-states are typically populated with 1%–2% of the total population of the nucleus. To isolate such a weakly populated

band from the strong γ transitions of the nucleus of interest and of all the competing reaction channels was impossible before the development of escape-suppressed Ge detector arrays.

3.5. The 4π γ-ray arrays GAMMASPHERE and EUROBALL

In the second half of the 1980s, when all the arrays described in Sections 3.2 and 3.3 had their success in producing exciting new experimental data, the nuclear physics community started to plan the next generation of γ-ray arrays. The goal was an ultimate 4π array of escape-suppressed Ge detectors to maximize efficiency. It became clear that the cost of such an array could not be financed by a single laboratory or a small collaboration. The result was the birth of two projects, GAMMASPHERE and EUROBALL. GAMMAPSHERE was proposed in 1987 as a national USA project of collaborating National Laboratories and Universities and the EUROBALL project started one year later as a collaboration of National Laboratories and Universities from six European countries. Extensive Monte Carlo simulations had been performed to prepare the final decision on the design of the two arrays. Before describing the two instruments the basic characteristics of an optimized γ-ray array are discussed.

Full-energy peak efficiency: The total efficiency of an array is limited by the efficiency of the individual Ge detector and the solid angle around the radiation source that can be covered with Ge detectors. The use of BGO escape-suppression shields limits the solid angle for Ge to ∼50%. An array of individual escape suppressed Ge detectors can have a maximum efficiency of 10%–12% at 1.3 MeV.

Peak-to-total ratio: The peak-to-total ratio is defined for a mono-energetic γ ray interacting with a detector as ratio of the counts in the full-energy peak divided by the total number of counts in the spectrum. With BGO shields this ratio can be 55%–65%.

Energy resolution: As discussed above the FWHM of a γ line of the energy 1.3 MeV measured with a Ge detector is $\Delta E \sim 2$ keV. In most in-beam experiments the line width is broadened due to the Doppler effect, plus scattering and slowing down in the target. A γ quanta of the energy E_0 which is emitted from a residual nucleus (moving with velocity v) and detected at an angle θ with respect to the beam axis is Doppler-shifted and its energy is given by:

$$E_\gamma = E_0 \left(1 + \frac{v}{c} \cos\theta\right). \tag{7}$$

Due to the finite opening angle $\Delta\theta$ of the detector the Doppler effect results in a broadening of γ line of:

$$\Delta E_\gamma = E_0 \frac{v}{c} \sin\theta \cdot \Delta\theta. \tag{8}$$

This broadening can be reduced by increasing the distance of the detector from the target and thereby reducing the opening angle for the detection. To keep the efficiency of the array constant more Ge detectors are required.

Other effects which contribute to the broadening of a γ line are the angular spread of the recoiling nuclei in the target and the variation of the velocity of the recoils due to the different loci of production in the target.

Isolated hit probability: A residual nucleus which was populated at very high spins will emit a cascade of 30 or more coincident γ rays. In order to identify such a long cascade a number of these transitions can be selected (f-fold gate). The fold f that can be used in practise will depend on the probability to detect f members of the cascade in different detectors (isolated hit

probability). Two γ rays interacting with the same detector mainly contribute to the background, the probability of summing both full energies is rather small. The isolated hit probability is enlarged with the granularity, which is the number of detectors in the array.

The optimization of a 4π γ array clearly depends on the experiment to be performed. For a low-spin experiment or for an experiment of very low or zero velocity of the recoils the granularity of the array can be much lower than for a high-spin experiment or for a low-spin experiment with high recoil velocities. In order to quantify the properties of an array for comparison the concept of the observational limit is introduced, that is defined as the weakest intensity of a line which can be separated from the background following the description of [43]. From the discussion above the observational limit will depend on the average separation of the γ lines in the spectrum SE_γ, on the FWHM ΔE_γ of a line, on the peak-to-total ratio P/T of the detector and on the coincidence fold f. The resolving power R of an array is defined as:

$$R = 0.76 \cdot \frac{SE_\gamma}{\Delta E_\gamma} \cdot P/T. \tag{9}$$

The factor 0.76 comes from the fraction of a Gaussian peak, which is included in setting a coincidence requirement or gate. The limit of observation α_0 depends then on the peak-to-background ratio of a spectrum of the fold f and on R

$$\frac{N_P}{N_b} \cdot f = \alpha_0 \cdot R^f \tag{10}$$

where $f - 1$ is the number of gates placed in the cascade, N_P the number of counts in the peak and N_b the number of counts in the background. With each higher fold condition the background is diluted in a matrix of higher dimension. In addition, triggering on the particles emitted in the reaction, the mass of the recoiling nuclei or the γ multiplicity reduces the background again. This further reduction is accounted for by another factor R_0

$$\frac{N_P}{N_b} \cdot f = \alpha_0 R_0 R^f. \tag{11}$$

With each higher fold or additional trigger the peak-to-background ratio is improved but also the number of counts in the peak is reduced. The limit of observation is reached when the number of counts becomes too small, e.g. <200 counts at a background of 1000 counts. The reduction factor of the peak count rate per fold depends on the efficiency of the individual Ge detectors and of the coverage of the sphere with Ge and thus on the total efficiency of the array. In summary, the dominating factors which determine the limit of observation of an array are the total absorption efficiency, the granularity of the Ge and the peak-to-total ratio.

The shape of a detector module. In the second generation arrays the total efficiency was maximized and the granularity increased. An optimum shape of the detector module consisting of the Ge detector and BGO shield had to be found to cover a 4π shell as complete as possible with detector modules. The answer to the problem had already been given by Archimedes. The simplest geometry to build a shell from regular polygons is the truncated icosahedron which consists of 20 regular hexagons and 12 regular pentagons. A higher granularity of the surface can be achieved with slightly irregular hexagons. The underlying symmetries lead to the "magic" numbers of detector elements: 32, 72, 122, ... For all these geometries only the number of hexagons increases while the number of pentagons 12 remains the same. Fig. 11 shows some of the geometries. Most of the 4π arrays described below use this scheme. The hexagons are filled

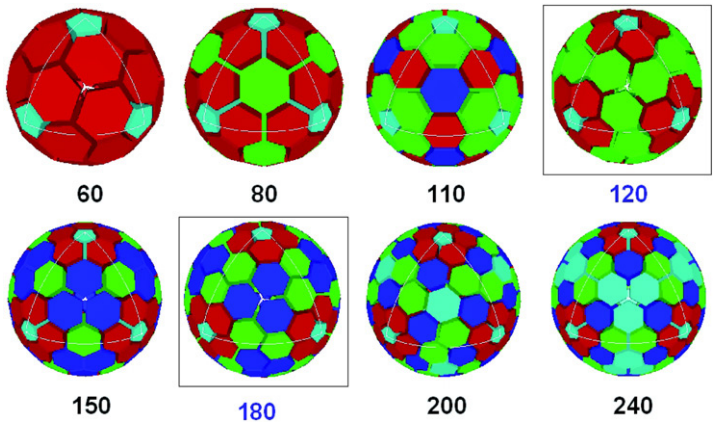

Fig. 11. The magic numbers of hexagons from the geodesic tiling of a sphere.

with detector modules using hexagonal BGO shields while the pentagons are used for the beam line and the holding structure of the array. Also, because of the thickness of the shell the detector modules cannot have a completely symmetric hexagonal shape but are slightly asymmetric.

3.5.1. GAMMASPHERE

While in Europe the development of a final state-of-the-art array happened in several steps including the development of new detectors, the physicists in the USA designed the array GAMMASPHERE in one step [44]. GAMMASPHERE used the magic number 110, i.e. 110 hexagons and 12 pentagons to tile the sphere. This number of elements was a very good compromise of sufficient granularity to detect high-multiplicity events and to keep the Doppler broadening small on the one side and reasonable cost on the other side. Each of the GAMMASPHERE modules which fills the 110 hexagons consists of hexagonal BGO shield and a cylindrical n-type Ge detector. Fig. 12 shows a side view of a GAMMASPHERE module. The distance between the target and the front face of the Ge detector is 25.25 cm. To achieve this distance the front 2 cm of the Ge detector is tapered with an angle of 7.45°. Nevertheless, the BGO shield is rather thin at the front part of the Ge detector. Therefore, events in the neighbouring BGO shields are also used to suppress Compton-scattered events. Each BGO shield has six optically separated elements, each with its own read-out. Only adjacent elements of neighbouring shields are used in the common suppression mode. Another interesting feature is the off-centre design of the cold finger in the cryostat. This allows the installation of a BGO detector behind the Ge crystal that suppresses Compton events scattered to forward angles and improves the low-energy background in the Ge spectra. Both features, the common suppression mode and the BGO back-plug contribute to the excellent P/T of ~0.68. The Ge detectors used in GAMMASPHERE have a relative efficiency of ~70%. These were the biggest n-type detectors which could be produced in a larger number at the end of the 1980s.

GAMMASPHERE started operating in 1993 with 32 detectors. Then, an important innovation was implemented, namely the longitudinal segmentation of the Ge detectors into two halves which was achieved by an electrical separation of the boron-implanted outer contact [79]. Due to the higher granularity the Doppler broadening of the γ lines was reduced and the energy resolution was improved from $\Delta E = 5.5$ keV to 3.9 keV at a recoil velocity of $v/c = 0.02$. GAMMASPHERE was completed in 1996 with 70 of the 110 Ge detectors being segmented.

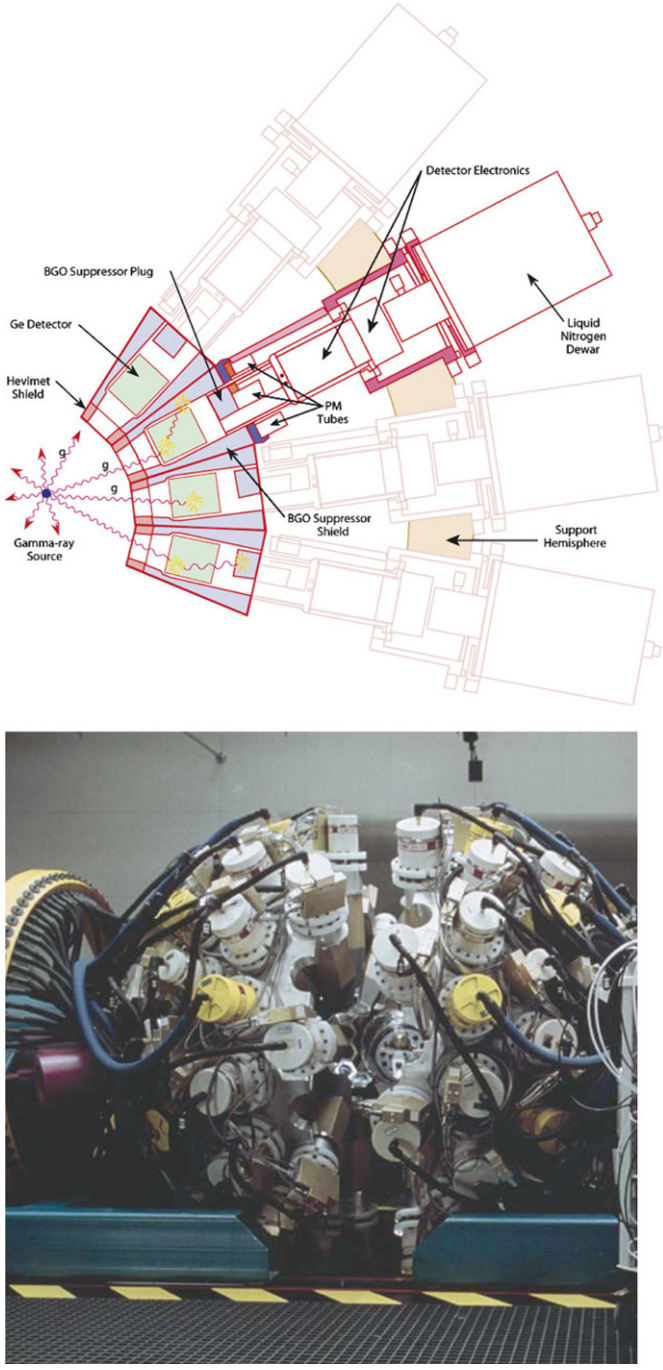

Fig. 12. Gammasphere at Lawrence Berkeley National Laboratory.

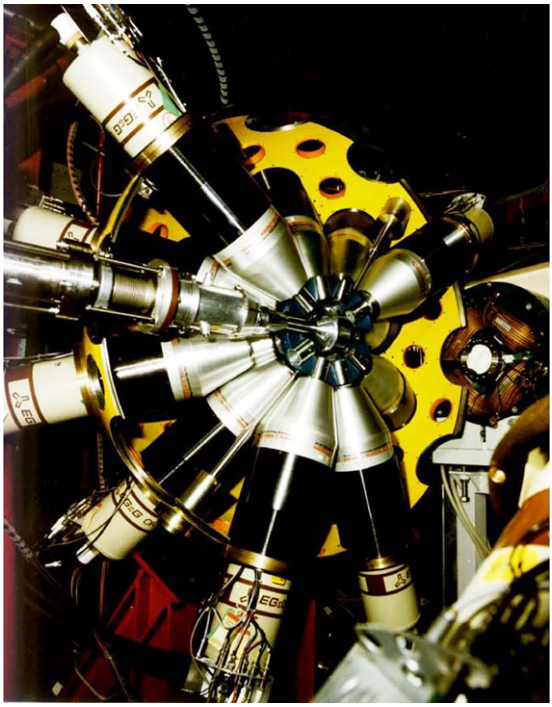

Fig. 13. GASP at the Legnaro National Laboratory.

In GAMMASPHERE 95% of 4π are covered with detector modules and the Ge detectors cover 46% of 4π. The fact that all detectors have the same shape and are arranged in a highly symmetric geometry is a big advantage for the data analysis.

The observational limit of GAMMASPHERE is further increased using ancillary detectors. Although this subject is beyond the scope of this article some have to be mentioned because of their importance. Microball [45] is an inner ball of 95 CsI(Tl) scintillation detectors covering 97% of 4π which was built at Washington University, St. Louis. Charged particles emitted in the reaction are identified by pulse-shape discrimination. Although the γ rays have to pass through the thin scintillators the efficiency and the P/T ratio of GAMMASPHERE are only reduced by $\sim$10% while the spectroscopy of the charged particles is a big gain for identifying reaction channels and cleaning the spectra. CHICO [46], built at the University of Rochester, is an inner ball of 20 segmented parallel plate avalanche counters (PPACs). It measures the direction of flight of the recoils which is needed for a full Doppler correction, e.g. in Coulomb excitation. Further ancillary detectors are the Neutron Shell, built at Washington University and the fragment recoil mass separator [47] at the Argonne National Laboratory.

3.5.2. The European arrays GASP, EUROGAM and EUROBALL

In Europe, the next generation of 4π arrays, GASP and EUROGAM1, began operating in 1992. GASP [48,49] which consists of 40 escape-suppressed Ge detectors (diameter 72 mm, length 80 mm) was built at the Legnaro National Laboratory, Italy. It has a sum-energy-multiplicity filter comprising an inner shell of 80 BGO scintillators which cover 80% of the solid angle. GASP can be operated in two configurations. The configuration I (with inner ball)

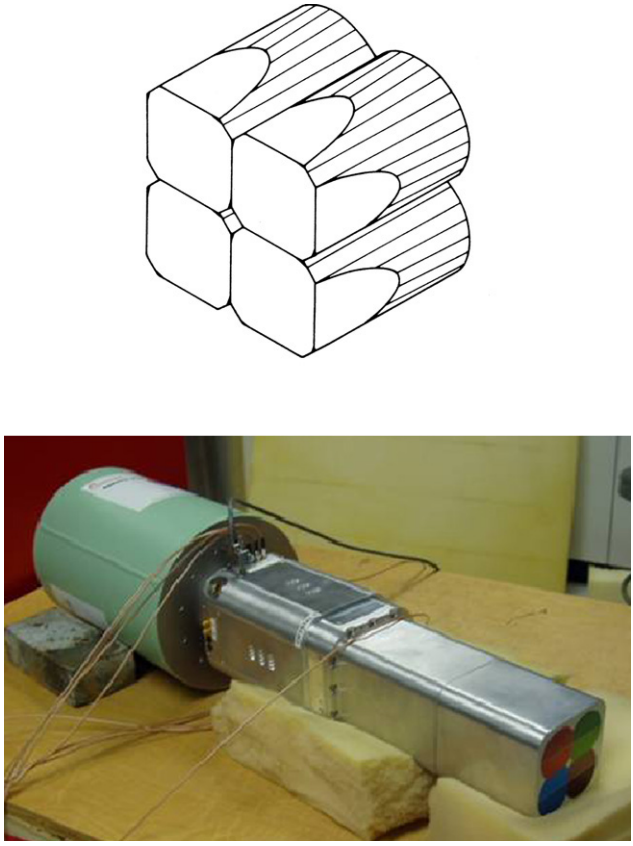

Fig. 14. The clover Ge detector. The top diagram is a schematic of the four Ge crystals.

has a full-energy peak efficiency of 3%, in configuration II (without inner ball) the Ge detectors are closer to the target increasing the solid angle and the full-energy peak efficiency is 5.8%. The gain in efficiency comes with a reduction of the resolving power R due to the larger Doppler broadening of the lines caused by the increased solid angle of the Ge detectors. Thus, the choice of the configuration depends on the specific experiment. GASP can be combined with a number of additional ancillary detectors: ISIS [50], a ball of 40 Si telescopes for the detection of charged particles, the recoil mass spectrometer CAMEL [51], a neutron detector array and a plunger device for lifetime measurements. Fig. 13 shows the inner part of GASP in configuration I.

EUROGAM I [52] was a UK–France collaborative project and operated at Daresbury Laboratory, UK. It used 45 escape-suppressed Ge detectors at a distance of 205 mm from the target yielding a full-energy peak efficiency of 5.6%. It was coupled to the Daresbury recoil mass spectrometer [34].

In parallel with the construction of these arrays a development programme was launched in order to enhance the granularity of future arrays. The limit of observation is essentially determined by the full-energy efficiency and the granularity (Doppler broadening, isolated hit probability) of an array. The full-energy efficiency of a 4π array of escape-suppressed Ge detectors is limited to 10%–12% by the available size of individual Ge crystal and by the maximum coverage of the sphere with Ge which is $\sim$50%. Increasing the granularity by a

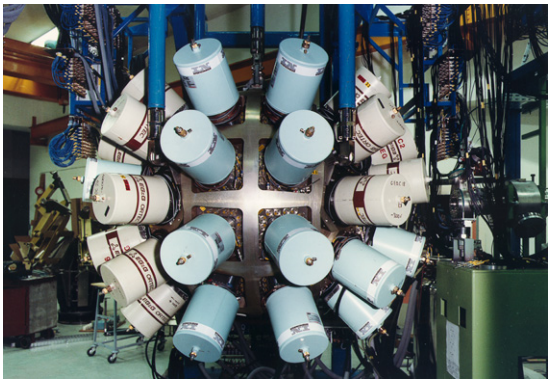

Fig. 15. Eurogam II at IReS Strasbourg.

larger number of Ge detectors positioned further away from the target is a too costly solution. GAMMASPHERE, with its 110 detectors, reached nearly the maximum efficiency, and as noted before the granularity was increased after the early implementation phase by segmenting the Ge detectors into two d-shaped parts. In Europe, another solution was chosen to increase the granularity, namely the composite detector. The clover detector [53] developed in collaboration between CRN-Strasbourg and Intertechnique (later to become Eurisys Mesures and Canberra France) was the first of these composite detectors. The clover detector shown in Fig. 14 consists of four closed-packed coaxial n-type Ge detectors. The outer faces are tapered to a rectangular shape in order to maximize the efficiency in a given solid angle. The individual Ge detectors are 50 mm in diameter and 70 mm in length before grinding to their final shape. The four tapered crystals have a total volume of $\sim$470 cm^3 which is 30% more than a GASP/EUROGAM detector. A further gain in efficiency is achieved by adding back the events Compton scattered between the four detectors into the full-energy peak. The measured relative efficiency of a clover detector is $\sim$130% which has to be compared with typically the efficiency of 70%–80% of a coaxial n-type detector. Thus, the clover detector not only improves the granularity by a factor of four but also the efficiency. Another important property of the clover detector is its sensitivity to the linear polarization of γ rays, which comes from the different intensities of events Compton scattered parallel or perpendicular to the reaction plane. Other advantages are the better timing and the reduced sensitivity to neutron damage due to the small-diameter crystals. The four Ge crystals of a clover detector are mounted in a common cryostat of a rectangular shape. With this shape, the clover detectors are not well-suited to cover a full sphere, but they have a very good geometry to be positioned in two rings close to 90° with respect to the beam direction. At 90° the Doppler broadening of the lines is maximal and at this position the clover detector can most effectively limit the broadening due to their granularity [54].

The EUROGAM II spectrometer comprised two rings of 12 clover detectors in suppression shields around 90° to the beam direction. The forward and backward directions each had 15 single-element Ge detectors of EUROGAM I. The single-element detectors were 205 mm and the clover detectors 230 mm from the target. The total coverage of the sphere with Ge detectors was 40% giving a total full-energy efficiency of 8.1% at 1.3 MeV. A photograph of the EUROGAM II is shown in Fig. 15.

The next significant development in detector technology was the production of a very large composite detector, the cluster detector. Seven n-type Ge detectors were grouped in a single

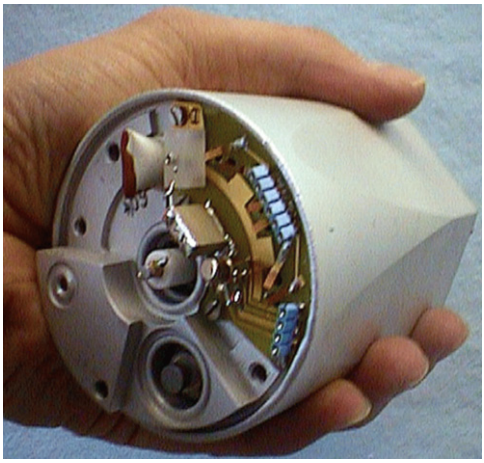

Fig. 16. Encapsulated Euroball Ge detector.

cryostat and surrounded by a BGO escape-suppression shield of a hexagonal shape, which was adapted to the polyhedron structure of a 4π array (the 60 geometry, see Fig. 11). For optimum add-back performance of Compton-scattered events the Ge detectors have to form a compact block with minimized space between the detectors. Cylindrical detectors are not well-suited for this purpose; therefore the first step was the development of a hexagonal tapered Ge detector. It could be shown that such a detector could be produced without loss in energy resolution and timing properties [21]. A more severe problem was the operation of seven hexagonal, closely packed Ge detectors in a common cryostat. The production yield of such a system was expected to be too low for a serial production at reasonable cost. In addition, there were doubts about the reliability and long-term stability of such a composite detector. The solution to this problem was the development of a hermetical encapsulation of Ge detectors by a collaboration of the University of Cologne, the company Eurisys Mesure and the KFA Jülich [55]. The final shape of the encapsulated Ge detector was optimized with Monte Carlo calculations. It is hexagonal at the front and circular at the rear of the capsule. The aluminium can has a thickness of 0.7 mm and the internal distance between the Ge surface and the can is 0.5 mm. When the capsule is mounted in the cluster cryostat the distance from Ge to Ge of two adjacent detectors is 2.5 mm. The Ge crystal has a diameter of 70 mm at the rear end and a length 78 mm, which yields a relative efficiency of $\sim$60%. Fig. 16 shows a photograph of an encapsulated detector.

The capsule is hermetically sealed by electron welding of the capsule lid and the feedthroughs. A getter material maintains the ultra-clean vacuum of the capsule in the full temperature range from 80 K to the annealing temperature of 105 °C. The capsule vacuum is separated from the vacuum of the cryostat. The encapsulation technology has several advantages: a contamination of the detector's surface is excluded even if the vacuum of the cryostat is broken; for annealing of neutron damage the capsule can be heated in an ordinary oven to 105 °C for 1–2 h; as the cold parts of the preamplifier are mounted on the capsule lid, they can be easily removed during annealing or for replacement. More than 150 encapsulated Ge detectors were produced for the EUROBALL project between 1992 and 1996. They have been annealed many times to remove neutron damage and still have their original energy resolution of $<$2.1 keV at 1.3 MeV. The failure rate of these detectors is $<$3% over the period of more than 10 years. Fig. 17 shows a

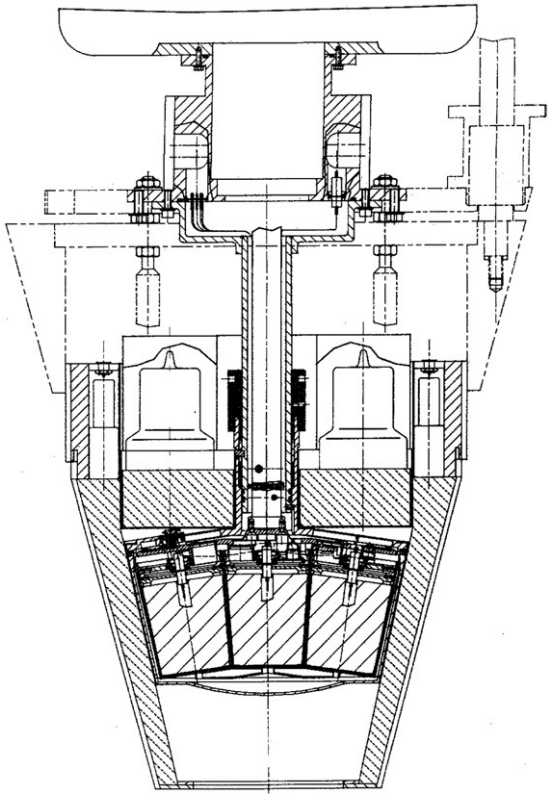

Fig. 17. Euroball cluster detector with BGO escape-suppression shield.

Fig. 18. The seven encapsulated Ge detectors of a Euroball cluster module.

Table 3
Cluster specifications at 1.3 MeV

Energy resolution in add-back mode	2.3 keV
Full-energy peak efficiency, ε_p	0.3
Peak-to-total (only Ge)	0.39
Peak-to-total with BGO shield	0.63
Add-back factor	1.44

schematic cross-section of a cluster detector and Fig. 18 a photograph of seven encapsulated detectors mounted on the cold finger.

The BGO shield consists of 18 optically separated elements, 12 elements surrounding the sides of the Ge detectors and 12 BGO plugs positioned behind the Ge detectors. The specifications of the cluster detector at 1.3 MeV are summarized in Table 3.

The cluster detector has an excellent efficiency at high energies due to the adding back of Compton-scattered events [56] and the high probability of absorption of the two 511 keV quanta in the case of pair production. For 10 MeV γ rays the spectrum measured with the cluster detector has almost the same quality as a spectrum measured with a large single detector at 1 MeV. This was demonstrated in nuclear resonance fluorescence experiments with the first cluster detector at the S-DALINAC in Darmstadt. The improvement of the peak-to-background ratio of the γ-ray spectra in the energy range up to 7 MeV excited by the $(\gamma,\ \gamma')$ reaction was impressive [57–59]. In the spring of 1994 six cluster detectors were assembled at the University of Cologne and used in two pre-EUROBALL campaigns at the tandem accelerator of the MPI-K Heidelberg and at the UNILAC of the GSI. In addition, a series of experiments were performed at the tandem accelerator at Risøin Denmark in the Pex (Pre-EUROBALL experiments) campaign. Only one of the setups of these experiments shall be mentioned in more detail here, the cluster cube as shown in Fig. 19.

The cluster cube consisted of six clusters arranged on the six sides of a cube at 11 cm from the target. This close packing is achieved by removing the BGO side elements of the suppression shield, see Fig. 17. In this geometry 65% of the solid angle was covered with Ge yielding a full-energy peak efficiency of 19% which is almost a factor of 2 larger than the efficiency of GAMMASPHERE and EUROBALL. The P/T is still 0.5 when using only the BGO back-plugs due to the high intrinsic P/T = 0.39 of Ge cluster. On the other hand, the solid angle of each of the individual 42 Ge detectors of the cluster cube is large resulting in a large Doppler broadening at higher recoil velocities and in a reduced isolated hit probability. Thus, the cluster cube takes full advantage of its high efficiency in experiments with low recoil velocities and low γ multiplicity. Examples include γ-ray spectroscopy in the super-deformed potential minimum of ^{240}Pu [60] and the study of the β decay of ^{98}Ag [61].

The detector array EUROGAM II was upgraded in 1997 with the addition of 15 cluster detectors to become EUROBALL III [62,63] and was operated at the Legnaro National Laboratory (LNL), Italy. It was built by a collaboration from France, UK, Germany, Italy, Denmark and Sweden. EUROBALL III consists of three sections, two end caps around the beam axis and a central section around 90°. In the backward end cap were the 15 Cluster detectors covering roughly 1π at 44.5 cm from the target. The photopeak efficiency of these detectors was 4.4%. The forward end cap, roughly 1π, comprised 30 escape-suppressed single Ge detectors from EUROGAM II, (with some Ge's from GASP). The Central section, covering 2π, comprised 26 clover detectors in suppression shields. These detectors were mostly at 26.5 mm from the target and had a photopeak efficiency of 3.8%. A schematic view of EUROBALL is shown

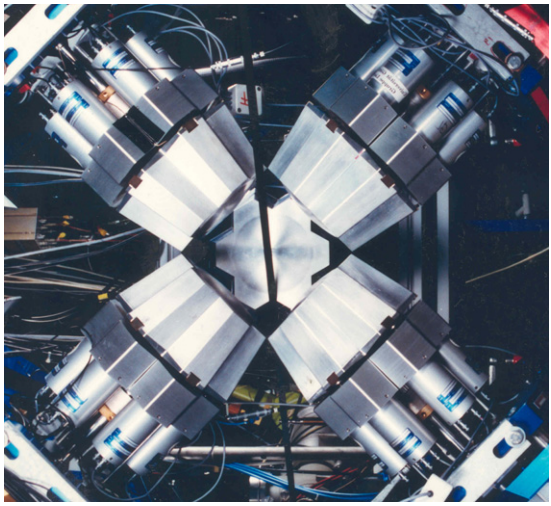

Fig. 19. The Cluster cube consisting of six Euroball cluster modules (one module was removed to take the photo).

in Fig. 20. Several ancillary detectors were coupled to EUROBALL III that further increased the resolving power. ISIS, a 4π array of 40 Si telescopes was used to detect charged particles emitted from the target. The forward end cap of single-crystal detectors could easily be removed and replaced by ancillary detectors. One of these was an array of 50 liquid scintillators for the detection of neutrons, called the neutron wall [64]. A plunger device for lifetime measurement [65] was installed as well as a setup for the measurement of g-factors. The full suite of ancillary detectors used with EUROBALL is summarized in [66].

After two years of operation at Legnaro EUROBALL was moved to the Vivitron accelerator at IReS Strasbourg, France where it was upgraded by an inner ball of 210 BGO detectors to become EUROBALL IV, shown in Fig. 21. By grouping the inner ball detectors, the Ge detectors and the BGO elements into 164 subgroups of equal efficiency and solid angle an excellent performance for the determination of the total γ-ray energy and the γ multiplicity could be achieved.

GAMMASPHERE and EUROBALL IV have similar efficiency and resolving power. The differences in their design and configurations lead to advantages and disadvantages for particular measurements. The big advantage of GAMMASPHERE is the high symmetry of the array, which facilitates the data analysis considerably. Advantages of EUROBALL are the high efficiency of the cluster part for high-energy γ rays and the high polarization sensitivity of the clover [54] and the cluster [67] detectors. The forward direction single Ge crystal spectrometers from Eurogam could easily be removed from the array without a big loss in γ efficiency and be replaced with ancillary detectors such as the neutron wall [64]. GAMMASPHERE explored the segmentation of Ge detectors and EUROBALL contributed with the development of composite detectors and encapsulated Ge detectors, which are the basis for the future complex composite detectors, see Section 4.

3.5.3. Impact of the large 4π arrays

The experiments with GAMMASPHERE and EUROBALL led to a tremendous gain in the knowledge of the nuclear structure at high angular momentum, high temperature and nuclei with exotic proton to neutron ratios. A compilation of the achievements can be found at [66,68].

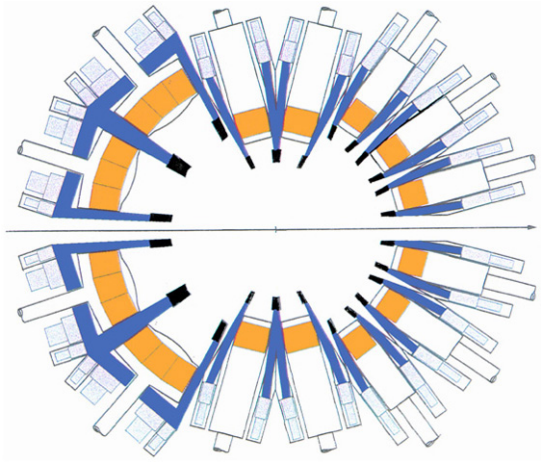

Fig. 20. A schematic view of Euroball with 15 cluster modules at backward angles, 26 clover modules around 90° and 30 individual Ge detectors at forward angles with respect to the beam direction.

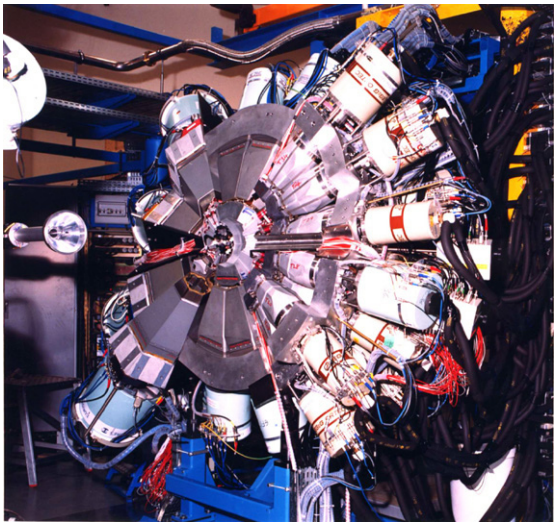

Fig. 21. The Euroball IV array at IReS Strasbourg (one-half of the array is pulled back for access to the target chamber).

GAMMASPHERE and EUROBALL are the culmination of 4π arrays with escape-suppressed Ge detectors. In order to increase the limit of observation by orders of magnitude a new approach to γ-ray detection and array design is required. This is discussed in the next sections.

4. Gamma-ray arrays with position-sensitive Ge detectors

The interest of nuclear structure physics is currently moving more and more to nuclei with extraordinary N/Z ratios close to the proton and neutron drip lines. It has been shown that more than 1000 unstudied nuclei can be produced with heavy-ion induced fragmentation reactions

(MSU, RIKEN, GSI) or with the ISOL technique (REX-ISOLDE, SPIRAL). New facilities for the production and acceleration of unstable beams are being planned in Europe (FAIR, EURISOL) and in the USA (FRIB). These facilities will allow a detailed study of a variety of phenomena, e.g. neutron skins, neutron halos and the melting of shell effects in neutron-rich nuclei, the effects of $T = 0$ proton–neutron pairing in self-conjugate nuclei up to ^{100}Sn and the detection of waiting points in the r- and rp-processes of the nucleo-synthesis. The new exciting experimental perspectives have triggered development programmes in Europe and in the USA for γ-ray arrays with several orders of magnitude improvements in resolving power compared with the generation of GAMMASPHERE and EUROBALL. The new concept in array design is based on γ-ray tracking in highly segmented germanium detectors. The idea is to surround the target by a 4π shell of 100–200 position-sensitive Ge detectors. Using digital electronics and pulse-shape analysis techniques it is possible to identify the energy, time and position of every interaction point of a γ ray as it interacts, scatters and is finally absorbed in the 4π ball. The full event can be reconstructed in software using the Klein–Nishina formula to realize an array with very high efficiency.

The concept of a 4π shell was discussed in the early days of the EUROBALL collaboration but the position-sensitive technology was not available then. Position-sensitivity of the detectors is achieved by both segmentation of the outer contact and by analysing the charge drift times within a segment and the mirror charges induced in the neighbouring segments.

The reconstruction of the track makes it possible to decide if the γ ray was emitted from the target and fully absorbed in the Ge shell. From Monte Carlo simulations a Ge tracking array is expected to have a high efficiency (maximum coverage of the solid angle with Ge detectors), excellent ability to correct the Doppler effects (angle of the emission of the γ ray determined from the first interaction point in the Ge shell) and a very good peak-to-total ratio (by distinguishing between fully and partially absorbed events).

Two γ-ray tracking arrays are in their first phase of realization in which the proof of principle will be demonstrated. These arrays are AGATA (Europe) and GRETA (USA). Before discussing the details and the status of the two projects a few intermediate steps towards γ-ray tracking will be presented.

4.1. First generation of Ge detector arrays for experiments at unstable ion beam facilities

The physics programme at the existing RIB facilities is mainly based on nuclear reactions leading to low γ multiplicity, e.g. Coulomb excitation of the exotic nuclei and transfer reactions in inverse kinematics. The intensities of the particle beams of interest are often $<10^3$ particles/s, but the velocity of the reaction products is high. Therefore, the experiments require a high γ efficiency of the detector array and a high granularity in order to improve the final resolution by Doppler correction. Several arrays have been designed to meet the experimental demands at the various facilities.

SeGA [69]. This array is in operation at the National Superconducting Cyclotron Laboratory at Michigan State University and consists of 18 highly segmented, cylindrical Ge detectors. Each detector has a 4-fold longitudinal segmentation and 8-fold transversal segmentation, the latter resulting in 10 mm thick slices. The γ rays enter the detector perpendicular to the detector axis so that the slice thickness defines the opening angle for the Doppler correction. As the segments are relative small, a γ ray will normally interact with several segments. For Doppler correction the assumption used is that the segment where most of the energy is deposited was hit first. At

a detector distance of 20 cm from target and for a recoil velocity of $v/c = 0.35$, the energy resolution is 20 keV for a 1.3 MeV γ ray and the total full-energy efficiency 2.9%.

EXOGAM [70,71]. The array was built for experiments at SPIRAL, GANIL by a collaboration of France, UK, Denmark, Finland, Sweden and Hungary. The EXOGAM project comprises an array of segmented clover detectors each housed in a modular BGO escape-suppression shield. The clovers contain four Ge crystals of 6 cm diameter (before tapering) and 7 cm length each of which is longitudinally segmented in four quadrants [73]. The full EXOGAM array consists of 16 clovers that can be arranged in various configurations. The BGO side elements of the suppression shields can be removed to increase the germanium efficiency. In this configuration the germanium crystals are 11.4 cm from the target and a full array of 16 clovers has a total photopeak efficiency 18% with a P/T = 0.45. The energy resolution for a γ ray of 1.3 MeV emitted from a nucleus moving with $v/c = 0.075$ is 14.9 keV. Fig. 22 shows a spectrum of γ rays after Coulomb excitation of ^{74}Kr measured with EXOGAM [72].

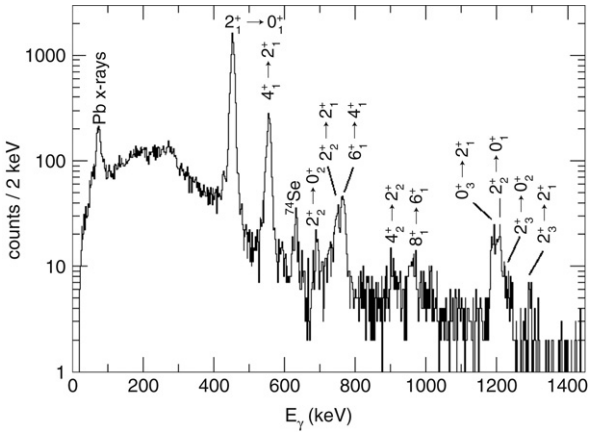

Fig. 22. Coulomb excitation of ^{74}Kr measured at SPIRAL with EXOGAM [72].

TIGRESS [74]. This array is being built at the TRIUMF laboratory in Canada. As in EXOGAM it uses 16 clover detectors. The individual Ge crystals are 6 cm in diameter and 9 cm long, each has a 4-fold longitudinal segmentation and one transversal segmentation, which gives a detector of 32 elements. An array of segmented Clovers is also operational at the HRIB facility in Oak Ridge [115].

MINIBALL. The MINIBALL array [75,76] was built by a collaboration between Germany and Belgium for experiments at REX-ISOLDE, CERN. The germanium detector development was a continuation of the concept of the EUROBALL cluster detectors. The full MINIBALL design consists of up to 40 encapsulated Ge detectors (32 were available in early 2007). They are arranged in 8 cryostats with 3 detectors and 4 cryostats with 4 detectors. The individual encapsulated Ge detector has the same shape as the detectors used for the EUROBALL cluster detector, i.e. it has a hexagonal shape at the front and circular shape at the rear with a length of 78 mm and a rear diameter of 70 mm. Each detector is longitudinally 6-fold segmented (through the centre of each side of the hexagon, see Fig. 23). Cooled input stages of the 7 preamplifiers needed to read out the core signal and the segment information are used, the 7 FETs and feedback components are mounted on the capsule lid in order to minimize microphonics. Again, encapsulation turned out to be a big advantage for complex composite detectors. One

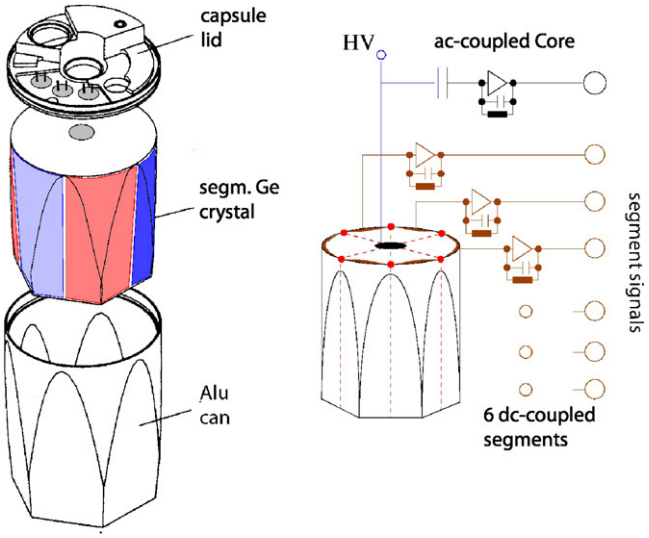

Fig. 23. The segmented MINIBALL detector.

reason is the increasing density of electronics where small mistakes in the wiring easily lead to oscillations of the preamplifiers and cross-talk between signals. With encapsulated detectors the cryostats can be easily opened and the electronics optimized without running the risk of damaging the Ge detector. The MINIBALL detectors have typically an energy resolution (at 1.3 MeV) for the core signal of 2.1–2.2 keV and of 2.3–2.5 keV for the segments, the loss in energy resolution for the segments is due to the additional capacitance between the Ge surface and the capsule wall.

All detector arrays described so far in this review use analogue electronics for signal processing. MINIBALL is the first Ge detector array with digital processing of the preamplifier signals. This allows pulse-shape analysis in real time to determine the interaction position of a γ ray within a detector segment. The resulting gain in granularity is more than one order of magnitude as will be shown below. Pulse-shape analysis requires a high bandwidth of the preamplifier and a good transfer function in order to conceive the full information of the detector signal. In addition, the need for a compact cryostat, housing up to 28 preamplifiers, places a constraint on the size of the preamplifier. A preamplifier fulfilling these demands has been developed by the University of Cologne and the MPI-K Heidelberg. Using SMD components the size could be limited to 25×40 mm. For pulse processing, MINIBALL uses the CAMAC module DGF-4C supplied by the company XIA, USA. Each single width CAMAC module comprises four Ge channels for energy spectroscopy and pulse-shape analysis.

The analogue part contains a gain adjustment via a 14 bit DAC and a Nyquist filter to limit the bandwidth for high frequencies. The signal is digitized by 12 bit, 40 MHz ADC and the results transferred to a FIFO and a FPGA (Field Programmable Gate Array). From the FIFO the trace can be read out to a host computer for off-line analysis or it can be analysed on-board by a DSP. The FPGA extracts the γ-ray energy in real time by a software filter; it can also be used with simple algorithms for pulse-shape analysis in real time. Four γ-ray singles spectra of 32 K length each can be stored in on-board RAM. A multiplicity bus and read-out with adjustable threshold, busy and synchronization lines and inputs for first- and second-level triggers make it possible to

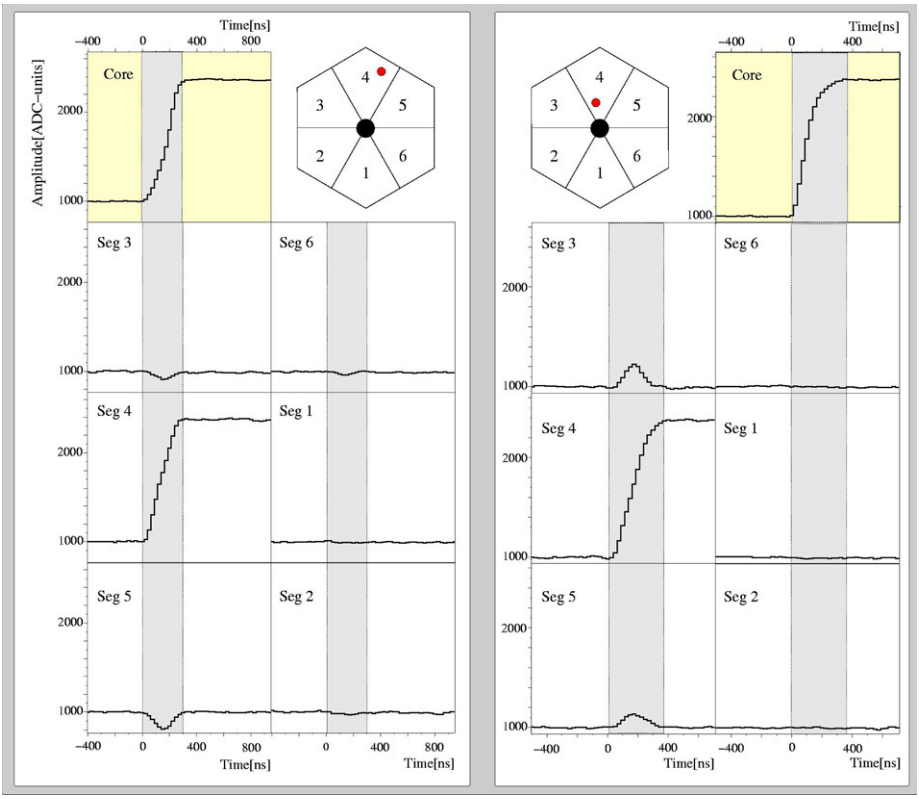

Fig. 24. Signals from a collimated ^{137}Cs source measured at the core and the six segments of a 6-fold segmented Miniball detector. Left figure: the γ ray was fully absorbed in segment 4 at a large radius (black point), right figure: the γ ray was fully absorbed in segment 4 at a small radius (black point).

incorporate the modules in a complex coincidence system. The energy resolution obtained with digital pulse processing compares well with the resolution measured with analogue spectroscopy amplifiers.

For the data analysis, the assumption that the segment where the largest energy is deposited was hit first, is made. This assumption is always valid if the γ ray interacts in the first step by the photoelectric effect. For energies $>$200 keV, an absorption via a chain of Compton scattering with a photoelectric effect as last interaction is more likely. In the case of small-angle scattering the assumption is still good as it leads to almost the same result for the determination of the angle of emission of the γ ray from the target. For large-angle Compton scattering and γ-ray energies $>$400 keV most of the energy is deposited in the first interaction and the Compton-scattered γ ray most likely interacts with a neighbouring segment or escapes the detector. In large-angle Compton scattering of γ rays $<$400 keV it is more unlikely that most of the energy will be deposited in the first interaction. However, in these cases the mean free path of the scattered γ ray is small and the next interactions will happen close to the first one. The analysis then averages over these interaction points.

The radial position of the main interaction is derived from the charge collection time of the electrons measured from the core signal. The current signal of the core, i.e. the derivative of

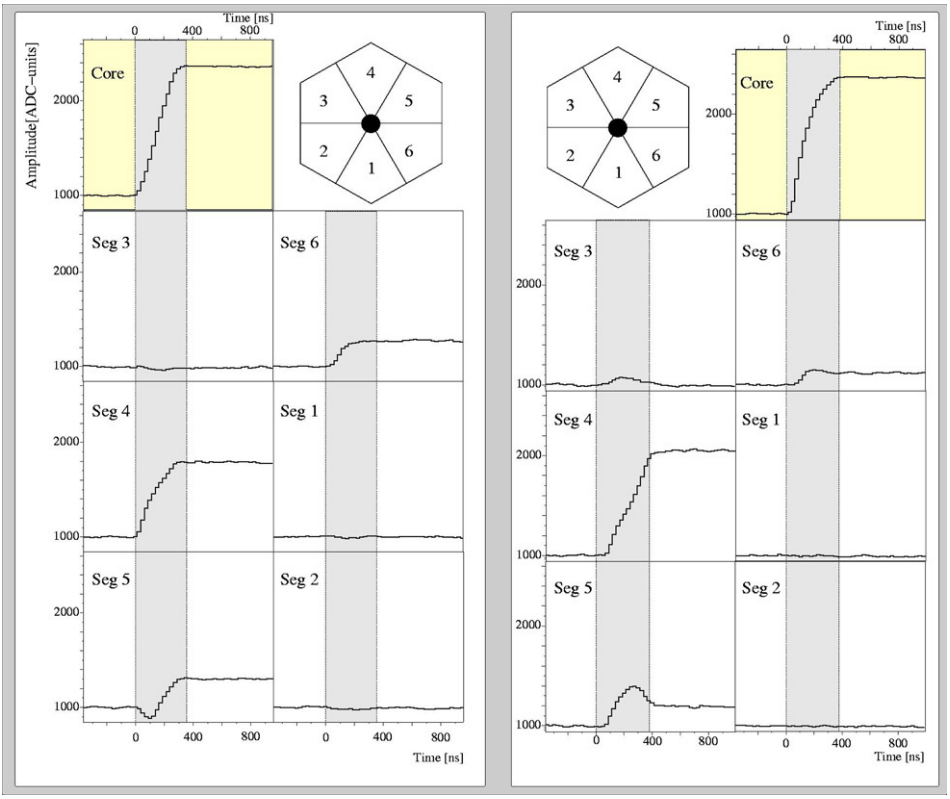

Fig. 25. Same as previous figure but in this case the γ ray is Compton scattered from segment 4 to segment 5 and 6 and fully absorbed in segment 6.

the charge signal, has its steepest slope at the time when all electrons are collected. This time is used to determine the radial position of the interaction. The azimuthal position of the main interaction within a segment is extracted from the amplitudes of the mirror charges induced in the two neighbouring segments. These mirror charges are only induced while the electrons and holes are moving in the segment with the interaction. Mirror charges and net-charges have very different pulse shapes. The net-charge pulse has a rise time given by the collection time of the electrons and holes and a fall time of 50 μs given by the time constant of the preamplifier. The mirror charge signal has its maximum pulse height while electrons and holes of the net-charge are moving and it returns to zero when all net-charges are collected. Thus, it is rather easy to deconvolute the mirror charge signal and the net-charge for the case of Compton scattering between neighbouring segments. The amplitude of the mirror charge signal also depends on the distance of the main interaction from the neighbouring segments and on the radial position of the main interaction. Mirror charge signals are positive for interactions close to the core where mainly holes are moving and negative for interactions in the outer part of the detector where the net-charge signal is dominated by the collection of electrons. If we calculate the quantity $A = (Q_l - Q_r)/(Q_l + Q_r)$, where Q_l and Q_r are the amplitudes of the mirror charge signals in the left and in the right neighbour, respectively, the effect of the radial position sensitivity cancels out in first order and A will only depend on the distance of the main interaction from

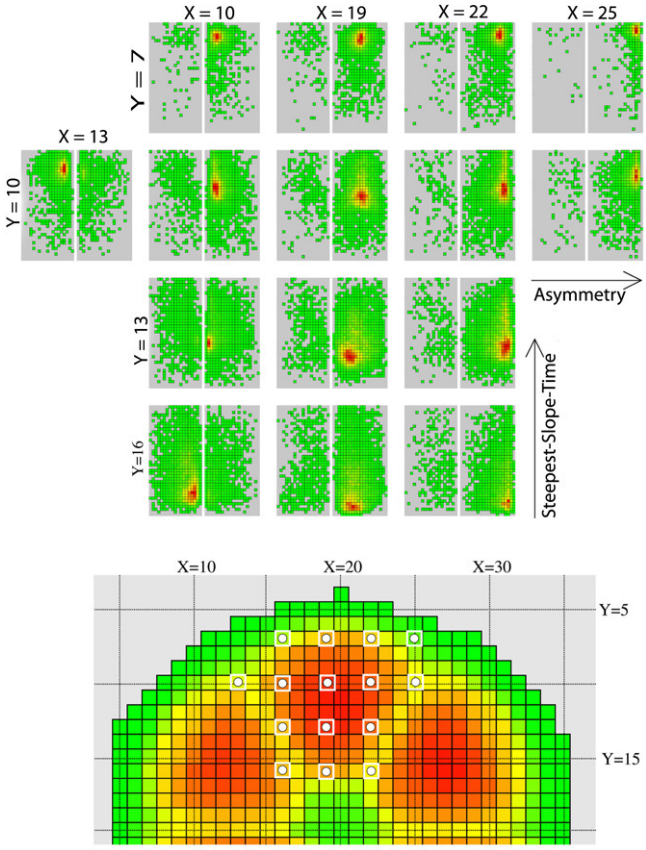

Fig. 26. Scan of one segment of a 6-fold segmented Miniball detector with a collimated ^{137}Cs source at 15 positions indicated in the lower part of the figure. In the upper part the steepest slope of the signals is plotted vs. the asymmetry of the mirror charge signals. For each position the matrix of the central segment and its left neighbour is shown.

the neighbouring segments. Therefore, A is used to determine the azimuthal position of the main interaction. Fig. 24 shows examples of the pulse shapes measured at the core and the six segments, respectively, for two selected interactions which were produced with a collimated ^{137}Cs source in segment 4. The signals of segment 4 have the same pulse height as the core signals, i.e. the whole energy was deposited in segment 4. In the right part of Fig. 24, the neighbouring segments show positive mirror charge signals, i.e. the main interaction occurred in segment 4 close to the core. The pulse height of the mirror charge in segment 3 is larger than in segment 5, i.e. the interaction in segment 4 occurred closer to its neighbour 3. In the left part of Fig. 24, the interaction occurred at a larger radius close to segment 5 as the mirror charge signals are negative and the signal of segment 5 is larger than the signal of segment 3. Fig. 25 shows two further examples of a collimated γ ray hitting segment 4 at a larger radius (left part) and close to the core (right part), respectively, and depositing the mainpart of the energy in segment 4. In both cases, the Compton scattered γ rays then interact with segment 5 by a second Compton scattering process and the scattered γ rays are finally absorbed in segment 6 by a photoelectric interaction.

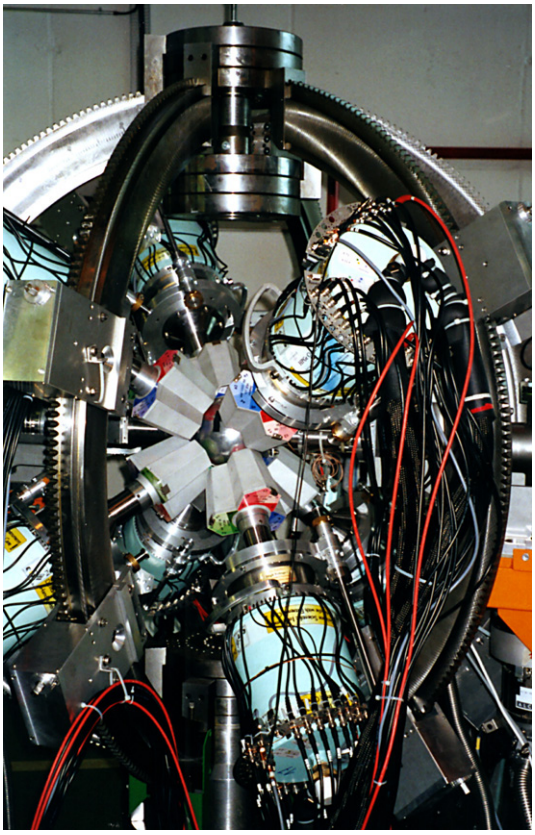

Fig. 27. The Miniball array at REX-ISOLDE, CERN.

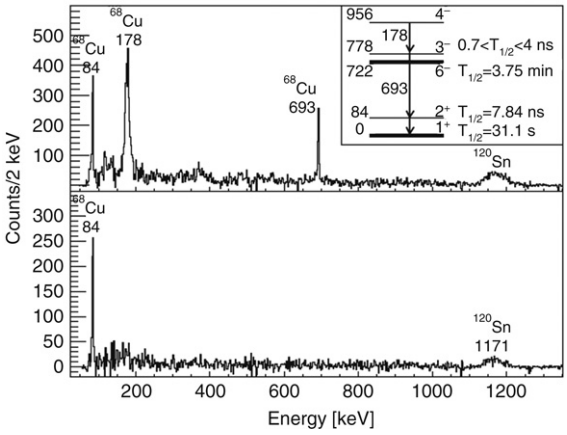

Fig. 28. Coulomb excitation of the 6^- isomer in ^{68}Cu [77] measured at REX-ISOLDE with MINIBALL.

The effective granularity of MINIBALL has been measured by scanning the front face of the 6-fold segmented detector in steps of 2.5 mm with a ^{137}Cs source collimated to 2 mm. The data

were analysed with the algorithms described above to extract the radial and azimuthal positions of the main interaction in two dimensions. The result is summarized in Fig. 26.

For the collimator positions indicated in Fig. 26, the time to the steepest slope of the current pulse of the core is plotted vs. the asymmetry A of the mirror charges. For each collimator position the matrices of the central segment and its left neighbour are shown. A survey of the results shows that it is possible to distinguish 16 collimator positions in one segment. Thus the effective granularity of one MINIBALL detector is enhanced from 6 due to segmentation to $6 \times 16 \approx 100$ due to pulse-shape analysis. With 40 detectors in MINIBALL there will be a granularity of 4000 compared with 170–240 of GAMMASHPERE and EUROBALL. The high granularity of MINIBALL has been verified experimentally by the energy resolution achieved after Doppler correction [75].

The MINIBALL cluster detectors are mounted on steel arcs that can be turned around the target making the instrument very flexible. The detectors can be moved along the arcs and the distance of the detectors from the target can be varied. Thus, it is easy to adapt the configuration to the demands of very different experiments with unstable beams and to combine MINIBALL with ancillary detectors. The specifications of MINIBALL are summarized in Table 4 for different configurations. Fig. 27 shows a photograph of MINIBALL at REX-ISOLDE where eight triple clusters are mounted at a distance of 12 cm from the target. In this configuration the efficiency is 8%. A spectrum from a recent experiment by Stefanescu et al. [77] is presented in Fig. 28. In this experiment, isomeric states in ^{68,70}Cu could be accelerated and Coulomb excited for the first time.

The last four MINIBALL detectors delivered by Canberra France are 12-fold segmented. In addition to the 6-fold longitudinal segmentation, they have one transversal segmentation at 1/3 of the crystal length. These detectors will further improve the position sensitivity of MINIBALL. A new technology for the electric contacts and the wiring of the segments had to be developed for these detectors, which was a major step for the production of highly segmented, encapsulated detectors needed for tracking.

Table 4
Specification of MINIBALL

	Coverage	No. of detectors	Distance from target (cm)	P_{Ph} (%)	FWHM @ 5% c		FWHM @ 15% c	
					At 90° (keV)	At 30° (keV)	At 90° (keV)	At 30° (keV)
Phase I	2π	18	13.5	5.1	3.1	2.3	7.3	4.6
	4π	18	9.5	10.3	3.9	2.6	10.1	6.2
Phase II	2π	40	18.5	6.4	2.7	2.2	5.6	3.7
	4π	40	11.5	16.5	3.4	2.4	8.6	5.3

5. The γ-ray tracking arrays AGATA and GRETA

In the late 1980s, when the GAMMASPHERE and EUROBALL array projects were launched, the construction of a shell consisting only of Ge detectors instead of using escape-suppressed individual or composite Ge detectors was being discussed, particularly in the EUROBALL collaboration. The efficiency for the full absorption of a 1.3 MeV γ ray would be considerably higher due to the increased coverage with Ge and because of the possibility to add back γ rays

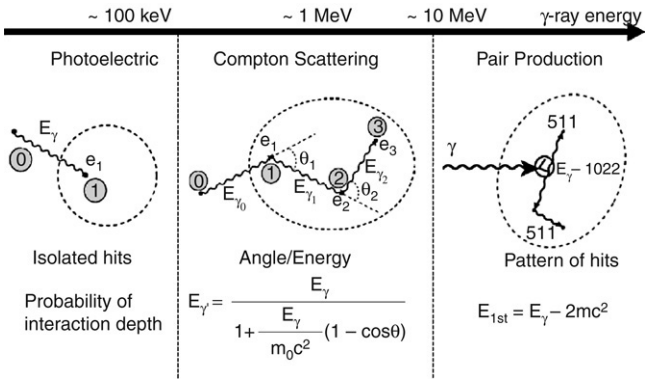

Fig. 29. The three most important γ-ray interactions for tracking.

that are Compton scattered between the Ge detectors to the full-energy peak. From Monte Carlo simulations an efficiency of 40%–60% of a Ge shell was predicted compared with ∼10% for GAMMASPHERE and EUROBALL. The problem of the Ge shell was to distinguish between two γ rays emitted from the target and detected in two adjacent detectors and one γ ray emitted from the target and Compton scattered to adjacent detectors. The only solution found was to increase the number of Ge detectors in the shell to 1000 or more in order to reduce the probability that coincident γ rays of high multiplicity interact with adjacent detectors. However, this solution was ruled out for cost reasons.

A completely new solution to the problem was proposed by the nuclear structure group at the 88-Inch Cyclotron of Lawrence Berkeley Laboratory a few years later, namely the concept of γ-ray tracking [78,79]. Tracking of a γ ray means measuring accurately the position, energy and time of all γ-ray interaction points in the Ge shell. The determination of the interaction points and the energies deposited at these points can be achieved with highly segmented Ge detectors and pulse-shape analysis. The sequence of a γ-ray scattering process is too fast compared with the time resolution of a Ge detector (∼5 ns) to be measured electronically. Therefore, tracking algorithms have to be used which are based on the underlying physical interaction processes.

- Gamma rays with energies below 150 keV interact with Ge predominantly by photoelectric absorption. Isolated interactions are assigned to a photoelectric absorption if the depth of the interaction point is consistent with the mean free path of a γ ray of the energy measured.
- In the energy range between 150 keV and ∼8 MeV the cross-section for Compton scattering is dominant. These γ rays are most likely absorbed by a sequence of a few Compton scattering processes and a final photoelectric interaction. In this case, for all possible permutations of the sequence of interactions the experimental scattering angle between subsequent events is compared with the angle calculated with the Compton scattering formula for the measured energies. The most likely sequence is identified by a χ^2-fit.
- For γ-ray energies of some MeV, pair production has to be taken into account. This process is characterized by a large energy deposited at an interaction point accompanied by one or two clusters of interactions points in the vicinity which are caused by the interaction of one or two γ rays of 511 keV created in the e^+e^- annihilation.

Fig. 29 illustrates the most important types of interactions. Uncertainties in the position determination of the interaction points limit the percentage of correct assignments of the

sequences. Good events will be lost and background events will be accepted. Thus, a good position resolution is crucial for the quality of a γ-ray tracking array. Simulations of such arrays show that the position resolution should be <5 mm and the energy resolution should be <3 keV [80–83].

Highly segmented Ge detectors. Several laboratories contributed to the development of highly segmented Ge detectors and explored their properties for three-dimensional γ-ray tracking. Closed-end coaxial detectors as well as planar detectors were studied. A group at Berkeley investigated in detail a 36-fold segmented detector [82,84]. This detector has a hexagonal, tapered shape and it is 6-fold segmented longitudinally and 6-fold transversally. The 37 FETs (1 for the core and 36 for the segments) are mounted in the cryostat and cooled for optimum energy resolution. In Italy, in the MARS project [85] a 25-fold segmented detector of a cylindrical shape with a 6-fold longitudinal segmentation, a 4-fold transversal segmentation and a small segment in the middle of the front face was tested. Again cold FETs were used to read out the 26 signals. In UK, in a Liverpool, Surrey and Daresbury collaboration [86,87], the properties of a 24-fold and a 36-fold segmented cylindrical detector with warm FETs were investigated. The encouraging results of all these studies can only be briefly summarized here. It was demonstrated, by scanning the detectors with collimated γ rays [84,85] and by Doppler correction of in-beam data [86,88] that a position resolution of 2–4 mm is feasible.

Planar Ge detectors are under investigation in a number of laboratories. Planar detectors can be highly pixellated or have double-sided strip structures of high density, which enables a good position resolution without performing a full pulse-shape analysis. The interaction depth in thicker planar detectors can be extracted from the charge drift times. With these properties, planar detectors are very well-suited for imaging applications. On the other hand, planar detectors are still built with guard rings at the edges, which are dead material for the radiation, and a large volume detector composed of planar slices needs a metal structure for mounting and cooling of the individual detectors. The unfavourable ratio of active-to-dead material hinders the application of planar detectors in an efficient 4π γ-ray array so far. Thus, it is a consensus that closed-end coaxial n-type Ge detectors are the best choice for building a 4π array.

The pilot projects in Europe and the USA have shown that tracking in principle is feasible. Experimentally, it has been demonstrated that a sufficient position resolution can be achieved. Extensive simulations of γ-ray tracking using the measured values of position resolution have been carried over a broad energy range and these predict that a 4π array of 100–200 detectors will have a sensitivity improved by several orders of magnitude compared with EUROBALL and GAMMASPHERE.

Given the importance of this development and its far-reaching implications, collaborations have been established in Europe and in the USA to construct 4π tracking arrays. The American project is called GRETA (Gamma Ray Energy Tracking Array) [78]. In Europe, a memorandum of understanding was signed in 2003 by 10 countries (recently two more countries have joined) to establish the AGATA (Advanced GAmma Tracking Array) [90–92] collaboration and the framework within which the project is organised. As a first step an AGATA demonstrator consisting of 15 Ge detectors will be built in order to prove the tracking principle experimentally. Also GRETA is starting with a sub-array of 30 detectors called GRETINA (Gamma Ray Energy Tracking In beam Nuclear Array). Both arrays are based on the results of the pilot projects and on the recent progress in Ge detector technology. It is no surprise that the design of the two instruments is basically very similar, but in detail different technical solutions are chosen. In this review, we will describe the constituents of AGATA in more detail, but we will point to differences with GRETA/GRETINA.

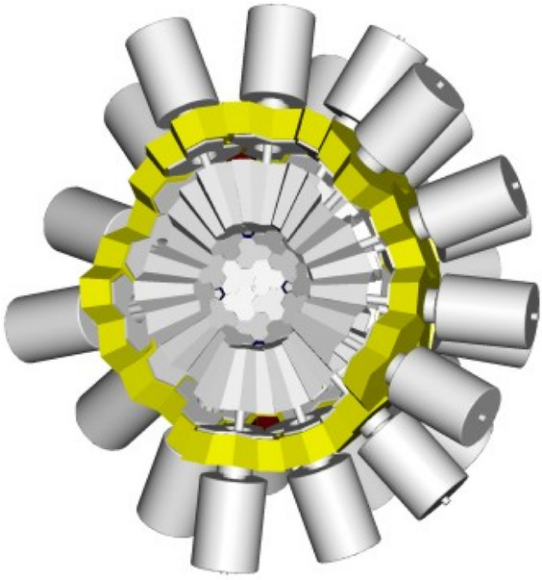

Fig. 30. A computer aided design presentation of the AGATA array.

5.1. The design and predicted performance of AGATA

AGATA is designed as a universal spectrometer for modern in-beam γ-ray spectroscopy. It will be used for experiments that produce both high and low γ multiplicity and for studies of stopped reaction products and those moving with very high velocity that can be up to $\beta \approx 0.7$. AGATA has to be able to run at very high rates, either because of high radioactivity or high beam intensities and sufficient inner space must be available to allow additional detectors to be installed.

The AGATA collaboration has investigated several options for the design of the spectrometer. Different numbers of coaxial detectors and groupings of detectors into cryostats have been considered for tiling the sphere with various numbers of hexagons and 12 pentagons, see Fig. 11. The performance of AGATA has been calculated using a Monte Carlo code based on GEANT4, which simulates the interaction of γ rays in the detectors and allows inclusion of realistic shapes and passive materials [93,94]. The chosen geometry is based on tiling the sphere with 180 hexagons and 12 pentagons. The configuration and proposed structure are schematically shown in Fig. 30.

In the chosen geometry the 180 hexagons are grouped into 60 identical triple modules or clusters of three slightly different asymmetric detectors. The 12 pentagons are not filled with detectors but used to bring the beam in and out and to support the structure. Table 5 summarizes the characteristics of the 180 detector geometry and Table 6 gives the calculated photopeak efficiency and peak to total at 1 MeV for various multiplicities.

It should be noted that the performance of a γ-ray tracking array depends strongly on the pulse-shape analysis and γ-ray tracking algorithms. Their development and optimization are a major part of the AGATA project and it is expected that these performance figures will improve. Nevertheless, Table 6 shows that the 180 detector spectrometer will have a very high efficiency and an excellent spectral response even at high multiplicities. The geometry has a

Table 5
The characteristics of the geometry of the 180 detector AGATA

Number of crystal shapes	3
Number of cluster shapes	1
Number of clusters	60
Solid angle coverage (%)	82
Amount of Ge (kg)	362
Crystal face to centre distance (cm)	23.5
Number of electronics channels	6660

Table 6
The predicted performance of the 180 detector AGATA at 1 MeV

Multiplicity	1	10	20	30
Efficiency (%)	43.3	33.9	30.5	28.1
Peak to total (%)	58.2	52.9	50.9	49.1

high granularity with an angular resolution of 1.25°, which will be very important for Doppler correction at high recoil velocities.

GRETA has chosen another interesting solution of tiling the sphere in hexagons and pentagons, namely 120 hexagons and 12 pentagons. In this case the detectors can be grouped into 30 cluster cryostats housing four detectors each with two different detector shapes. Due to the smaller number of detectors the inner diameter of GRETA is smaller than that of AGATA.

5.2. The AGATA Ge detectors

The detectors of AGATA are 36-fold segmented coaxial Ge crystals. The crystals have a length of 9 cm and a diameter of 8 cm at the rear and at the front they are tapered to a hexagonal shape with a 8° tapering angle. The 6-fold longitudinal segmentation goes through the middle of each flat hexagonal side. The 6-fold transversal segmentation forms slices of 8, 13, 15, 18, 18, 18 mm starting at the hexagonal front face of the detector. The thicknesses of the slices have been optimized by GEANT4 calculations for uniform distribution of the interactions and optimal pulse-shape sensitivity. Each crystal is encapsulated into a thin Al can using the technology developed for the Euroball cluster and the 12-fold segmented MINIBALL detector, which is described in the previous chapters. Fig. 31 shows the segmentation scheme and a photograph of an encapsulated AGATA detector.

The AGATA collaboration has received three symmetric encapsulated detectors from the company Canberra Eurisys, France and has placed orders for asymmetric detectors of the final shape for the 180 detector configuration for the AGATA demonstrator. The three symmetric capsules have a 10° tapering angle and the shape identical to that of the first detectors purchased by the GRETINA project [89]. In both projects, the purpose of the symmetric detectors was to study the properties of the 36-fold segmented detectors and a triple cluster as a basis for a final decision of the details and the configuration of the full instrument. All AGATA detectors have been tested in a test cryostat equipped with MINIBALL preamplifier (cold FETs) at the University of Cologne. The performance of the detectors is very encouraging. For the symmetric detectors the measured energy resolutions are 0.9–1.1 keV at 60 keV and 1.9–2.1 keV at 1.3 MeV for the 36 segment signals. For the core signals the energy resolution is 1.2 keV at 122 keV and 2.1 keV at 1.3 keV. The first asymmetric detectors delivered so far are on average ∼100 eV worse

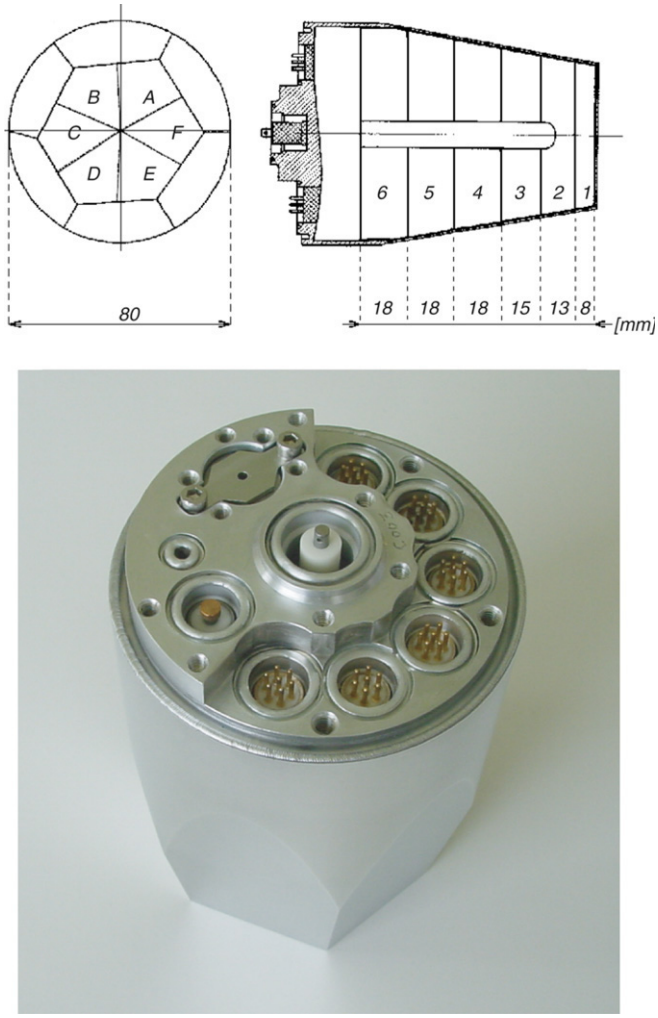

Fig. 31. The 36-fold segmented, encapsulated AGATA Ge detector.

in resolution but all measured values are well within the specifications required. The cross-talk between the 37 signal chains of each detector has been measured using digital electronics and then analysing all combinations of 2-fold coincidences. For all detectors the measured cross-talk is below 10^{-3}.

The AGATA cryostats. The design of the AGATA cryostats is based on the cryostats developed for the EUROBALL and MINIBALL cluster detectors. For all three projects cooled input stages of the preamplifiers are used with a good shielding between the input stages in order to minimize the cross-talk. While for EUROBALL and MINIBALL the FETs are cooled together with the detector by one cold finger connected to the LN_2 dewar, the AGATA cryostats have a separate cooling for the detector and the cold part of the electronics. The reason is the high power consumption of the electronics. Although each FET has only a consumption of ∼20 mW, the total consumption of the 111 FETs in an AGATA triple cluster adds up to 2.3 W. With separate cooling

Table 7
Specification of the AGATA preamplifiers

Property	Value	Tolerance
Conversion gain	110 mV/MeVN/Z (terminated)	±10%
Noise	0.6 keV FWHM 0 (pF)	
Noise slope	12 ± 2eV/pF	
Rise time	15 ns ± 2 ns (0 pF)	
Rise-time slope	∼ 0.3 ns/pF	
Decay time	50 μs (segment)	±5%
	30 μs (core)	
Integral non-linearity	<0.025% ($D = 3.5$ V unterminated)	
Output polarity	Differential, $Z = 100\ \Omega$	
Fast reset speed	∼10 MeV/μs	
Inhibit output	TTL	
Power supply	±6V, ±12V	
Power consumption of input FET	<20 mW	
Power consumption (except diff. buffer)	<250 mW	
Mechanical dimension	<70 mm × 50 mm × 7 mm (segment)	
	<55 mm × 50 mm × 7 mm (core)	

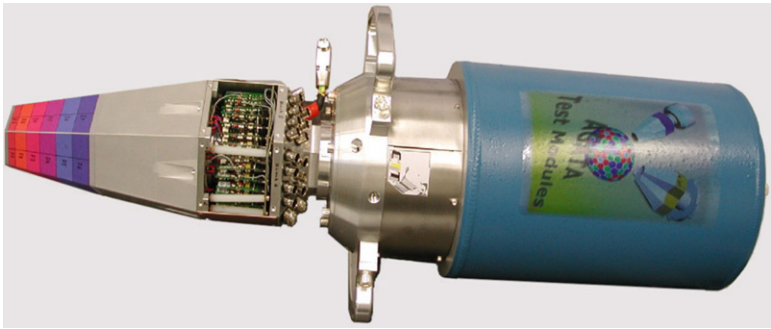

Fig. 32. Test cryostat for the AGATA Ge detectors.

it is much easier to operate the detector at ∼90 K and to adjust the temperature of the FETs to ∼130 K where their noise contribution is minimal. New preamplifiers have been developed by a collaboration of GANIL, the University of Milan and the University of Cologne [18,19]. They are optimized for good signal-to-noise ratio at fast rise times and for an unperturbed transfer function. Three segment preamplifiers are integrated on one PCB. The core preamplifier includes an on-board precision pulse generator that injects a test pulse via a 1.8 Ω resistor at the source of the core FET and then it is distributed through the bulk capacitance of the detector to all segments. The specifications of the preamplifiers are summarized in Table 7.

The AGATA cryostats are provided by the company CTT, Montabaur, Germany. A triple cryostat for the three symmetric detectors as well as test cryostats for individual detectors has been delivered. The test cryostats are used to characterize the first AGATA detectors in different European laboratories. Fig. 32 shows the test cryostat used for detector acceptance tests and Fig. 33 the symmetric triple cryostat in a first in-beam experiment at the tandem accelerator of the University of Cologne.

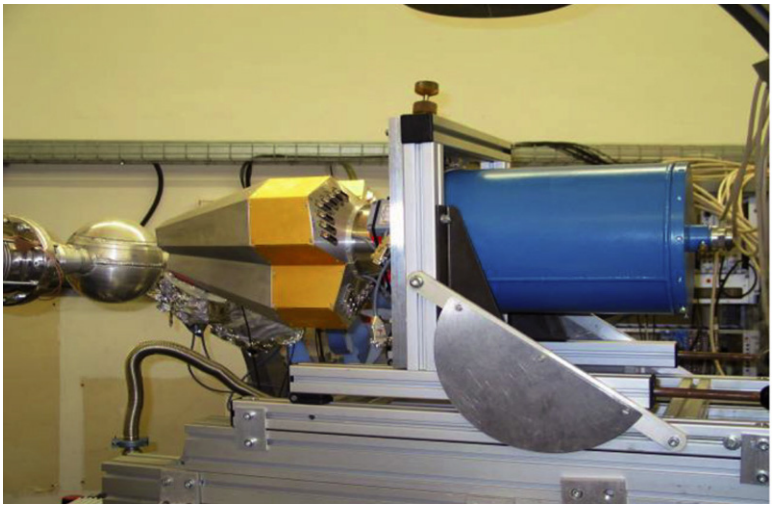

Fig. 33. The AGATA triple cluster at the Cologne tandem accelerator.

5.3. Data processing

AGATA requires a state-of-the-art and purpose built digital electronics and associated data acquisition system to process the signals from the Ge detectors. The full system has to cope with over 6000 channels with the rate of each possibly up to 50 kHz. A schematic diagram of the system architecture is shown in Fig. 34.

The segmented detectors provide 37 signals (36 outer contacts, 1 core contact) from the FET/ preamplifiers. The principle of the AGATA electronics is to sample these outputs with fast ADCs to preserve the full signal information in a clean environment so that accurate energy, time and position can be extracted. The first stage of the electronics will be a digitizer card located close to the detector. The digitizer contains 100 MHz 14 bit ADCs to digitize the signal and then the information is transmitted via an optical link to a "remote" pre-processing card. This card performs digital signal processing that is local to a particular detector such as energy determination and time. These cards transmit their outputs to the pulse processing part of the system which will be a farm of computers. This farm assembles the full data from all elements of the array, uses PSA algorithms to determine the position of the interactions, performs tracking to reconstruct the events and assembles the resulting data for storage. The whole system shares a global time reference (clock), which is supplied by a global trigger and synchronization control system, which is distributed by a network of optical fibres to the front-end electronics of each crystal. The first prototype cards have been tested and the full electronics for the AGATA demonstrator is expected to be available in 2008.

5.4. Development of algorithms for pulse-shape analysis and tracking

The performance of the γ-ray tracking arrays will strongly depend on the capability of the pulse shape and tracking algorithms. The task is not only to identify the individual interaction points of multiple interactions of the γ ray with the detectors with an accuracy of a few millimetres and a low percentage of errors, but also to find algorithms which are fast enough for real-time application with a computing power available in the near future. Intense research is

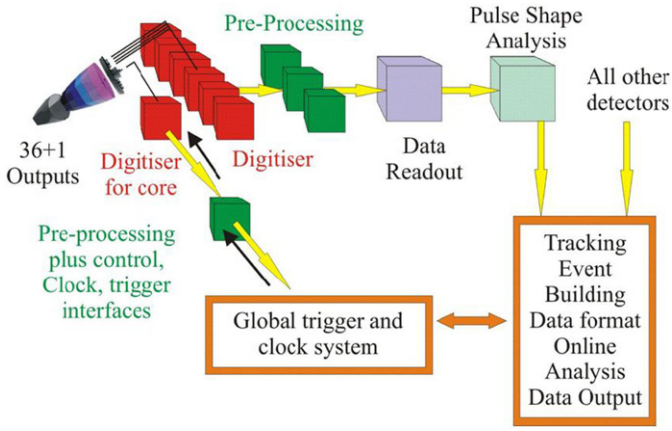

Fig. 34. Architecture of the AGATA digital electronics and data acquisition system.

going on in this field and encouraging results have been reported [82,85,86]. It is expected that the performance of tracking arrays will continuously improve over years based on an interplay of refined algorithms and increasing computing power. It is not possible to discuss the details of the different approaches and their constraints, however, most of this work is based on a few common procedures. As a first step a basis of the detector response has to be created, i.e. the pulse shape of the signals as function of the energy deposited at points defined by a regular grid inside the crystal is required. Any observed signal corresponding to multiple interactions in the crystal can be expressed as a linear combination of the basis signals where the coefficients are the energy deposited. The best basis system would consist of the measured detector response for each crystal. However, the measurement of the full characterization of one highly segmented detector is very time consuming. Therefore, the response of the detector has to be calculated. By solving the Poisson equation for the geometry of the detectors and the boundary conditions the electric field can be obtained. The concept of weighting field is used to calculate the transient charge signals. The charge carrier trajectories and the signals are calculated from the electric field in the detector taking into account the mobility of the electrons [95,96] and holes [97] and the crystal orientation. Application of the Ramo theorem [98,99] provides the charge recovery at the contacts. MGS (Multi-Geometry Simulation) is one of the computer codes used to calculate the detector response for AGATA [100]. In the second step the experimental data are compared with the basis in order to determine the coordinates of the interaction points. A gamma ray will normally have a chain of interactions in the shell of Ge detectors (e.g. 3–4 at 1.3 MeV). There can be more than one interaction in one detector segment or/and the γ ray is scattered to another segment of the same crystal or to an adjacent detector or even across the shell. Several fitting procedures have been developed in order to decompose the measured signals into the given basis signals, e.g. genetic algorithms [81,85,102], wavelet decomposition and a matrix method [101]. In the third step a tracking algorithm is applied in order to disentangle the coincident interaction points and to determine the total energy and the emission direction of those γ rays that have been fully absorbed in the Ge shell. Mainly two types of tracking algorithms have been studied so far: back tracking [103–105] and forward tracking [80,106,107]. The back tracking algorithm starts with the reconstruction from the last interaction, which is a photoelectric interaction of a fully absorbed γ ray. The energy deposited in this final photoelectric interaction is most probable in the energy range of $\sim$100–250 keV, independent of the energy of the incident γ ray. The forward

Fig. 35. An AGATA detector on the Liverpool scanning table.

tracking algorithm starts with the assignment of the coincident interaction points to clusters in a (θ, ϕ) space. This clustering of interaction points was found in Monte Carlo calculations due to forward peaking of the Compton scattering cross-section and the decreasing mean free path of the photons with decreasing energy. It has been shown [83] that back tracking can reconstruct events that are missing in forward tracking and vice versa. Therefore, a combination of both methods can increase the tracking efficiency. A third type of tracking algorithm which has been tested successfully is based on fuzzy logic [108].

5.5. *First experimental results*

The position response of the first 36-fold segmented, encapsulated AGATA detectors has been studied with radioactive sources and in-beam experiments. At the University of Liverpool, the symmetric AGATA detectors have been scanned with a 920 MBq ^{137}Cs source collimated to 1 mm along 16 linear and 17 azimuthal lines [109,110]. The principle of the scanning procedure is shown in Fig. 35.

A single Compton interaction in the Ge detector where the γ ray is scattered to 90° is selected by a coincidence between the Ge detector and a BGO scintillator, which identifies the scattered γ ray. The interaction point in the Ge detector is defined by the collimation of the source (1 mm) and a collimation slit (1.5 mm) in front of the BGO detectors. The condition that 374 keV has been deposited in the Ge detector and 288 keV in the BGO detector selects a single Compton scattering event. The measurements are very time consuming; scanning only half of the detector and requiring good statistics (>100 counts in the 384 keV line) in the segments of the three front rings takes around two months. The full data analysis and the comparison with the calculated detector response are in progress. A position resolution of 1–2 mm has been extracted so far from the data.

The first in-beam experiment with an AGATA detector has been performed in 2004 at the tandem accelerator of the University of Cologne. Details of the experiment are given schematically in Fig. 36.

The 2^+ state in ^{38}Ar was populated via the reaction d(^{37}Cl, n)^{38}Ar at a ^{37}Cl beam energy of 70 MeV and using a deuterated Ti foil as target. The recoil velocity of the ^{38}Ar ions was $v/c = 0.056$. The 2168 keV ground-state transition in ^{38}Ar was measured with the first

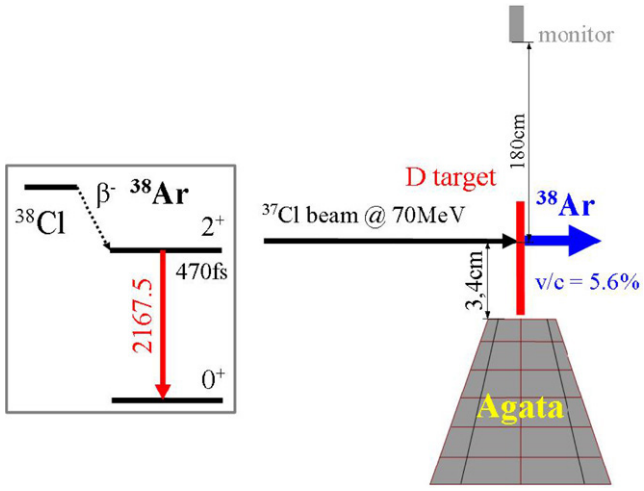

Fig. 36. Some details of a first in-beam experiment with an AGATA detector.

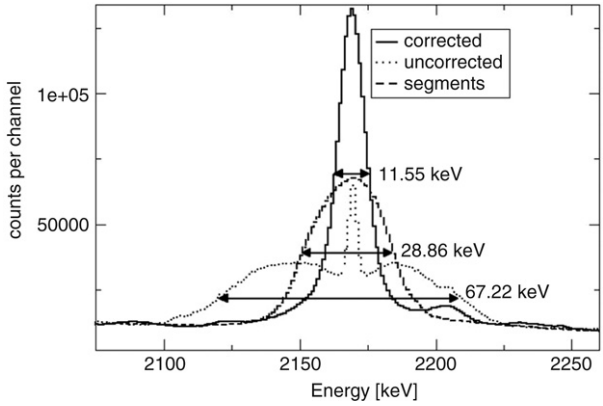

Fig. 37. The shape of the 2167.5 keV line in ^{38}Ar measured with a 36-fold segmented AGATA detector: dotted line indicates no Doppler correction, broken line indicates Doppler correction with segment information, solid line indicates Doppler correction with pulse-shape information.

symmetric, 36-fold segmented AGATA detector positioned at 90° with respect to the beam axis and at a distance of 3.4 cm from the target. The aim of the experiment was to extract an average position resolution of the AGATA detector from the line width of the 2168 keV transition. The results are presented in Fig. 37.

The line width is 67.2 keV if the segmentation and the pulse-shape analysis are not taken into account. The narrow peak on top of the Doppler broadened structure is caused by the γ decay of ^{38}Cl which is produced by the competing reaction d(^{37}Cl, p)^{38}Cl. Using the segment information for the position of the first interaction point in the detector reduces the line width to 28.9 keV. Applying in addition a pulse-shape analysis for each event with the same simple algorithms described in chapter 4.1 for the 6-fold segmented MINIBALL detectors reduces the line width to 11.6 keV. The contribution of the reaction kinematics was estimated with a monitor detector positioned at 180 cm distance from the target to be 5.8 keV. The Doppler shift depends

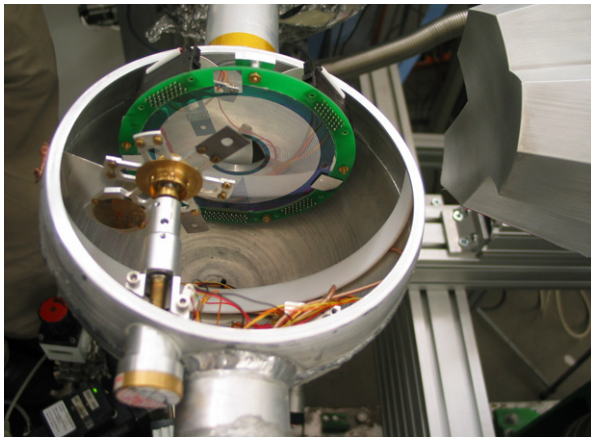

Fig. 38. Target chamber with the Si detector and AGATA triple cluster (right-upper corner).

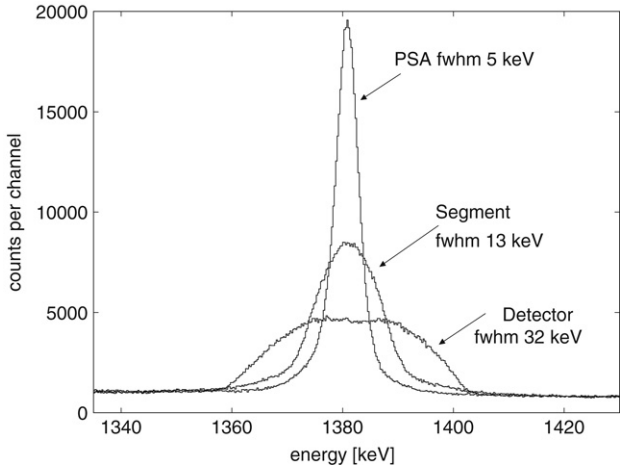

Fig. 39. Results of the Doppler correction of the 1382 keV transition in ^{49}Ti from segment information and pulse-shape analysis (PSA).

only on the angle of detection of the γ ray with respect to the beam axis. Therefore, the width resolution can be deduced and was found to be 4.3 mm [88].

The properties of the first AGATA triple cluster were also studied in-beam in 2005. Again the position sensitivity of the detector was used to reduce the Doppler broadened line width and to calculate the position resolution. The reaction chosen was d(^{48}Ti, p)^{49}Ti, the 100 MeV Ti was provided by the Cologne tandem accelerator. The recoil velocity of the ^{49}Ti ions was $v/c = 0.06$–0.07. The emission angle of the protons was measured with a double-sided silicon strip detector which was segmented into 32 rings on one side and into 64 sectors on the other side. A photograph of the experiment is shown in Fig. 38. The data are being analysed by several European groups testing different pulse-shape algorithms. Preliminary results achieved by the Padova group with the grid method are presented in Fig. 39. By pulse-shape analysis the line

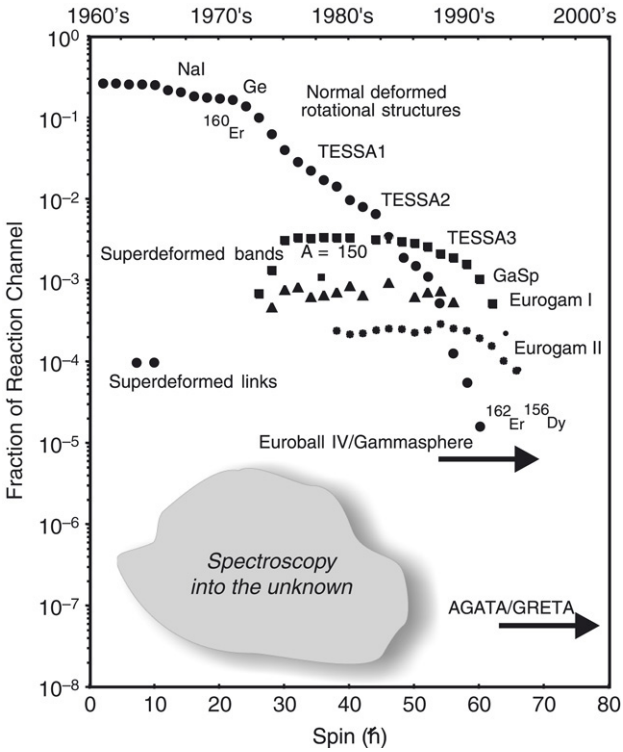

Fig. 40. The sensitivity of γ-ray arrays measured by the fraction of the reaction channel that can be observed as a function of spin for some selected nuclear structure phenomena. The associated timeline and arrays are indicated.

width of the 1382 keV line in ^{49}Ti could be reduced from 32 to 5 keV which corresponds to a position resolution of 4.4 mm [111].

In the USA, the GRETINA project is also progressing very well. In-beam tests have also been performed with a single crystal and a triple module at Berkeley and MSU. A position resolution of $\sim$2 mm RMS has been reported [112]. Recently, a first quadruple cluster has been delivered by Canberra France. Because of the large number of 148 high-resolution channels in a quadruple cluster, and ease of repair, the American collaboration decided to use warm FETs for the segment preamplifiers and to cool only the four core FETs in the vacuum of the cryostats in order to obtain an optimum energy resolution for the core signals. AGATA and GRETINA will have made considerable progress at the time this article will be published. The interested reader can always find the actual status at the home pages of the two projects: AGATA at http://www.gsi.de/agata/ and GRETINA: at http://grfs.lbl.gov.

6. Conclusion

Germanium detector technology has played a vital role in nuclear structure physics and its discoveries. The most important steps in the development from the Ge(Li) detector to the upcoming γ-ray tracking arrays have been reviewed. Fig. 40 summarizes the impressive achievements as a function of time and array development. The figure shows the sensitivity to detect a fraction of the reaction channel as function of the spin for some selected nuclear structure

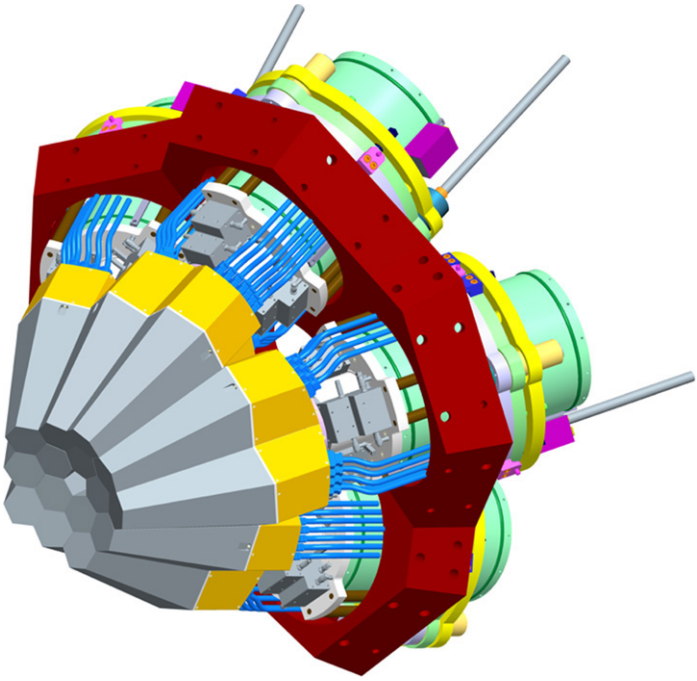

Fig. 41. A computer aided design image of AGATA with 15 detectors (3 triple modules) that will be operated in 2008 in Legnaro National Laboratory.

phenomena. The sensitivity improves almost quadratically with time and will have reached seven orders of magnitude with the expected specifications of the γ-ray tracking arrays.

The feasibility of γ-ray tracking still has to be proven experimentally, however, important progress has been achieved. It has been shown that the interaction points of multiple scattering in a Ge detector can be identified with a position resolution of a few mm.

With its massive increases in resolving power and efficiency AGATA and GRETA will permit access to the furthest reaches of the nuclear chart. The study of the structure at the very limits of nuclear stability is crucial in order to answer some of the most pressing questions in the field. These include the isospin dependence of the effective nuclear interaction, the ability to explain collective phenomena from the properties of the individual nucleons and the limits of nuclear existence and indeed Mendeleev's table of elements. In the last decade, it has become clear that many of our preconceptions of nuclear structure have to be revised. Nuclear radii are not always proportional to $A^{1/3}$; instead, neutron-rich nuclei develop a diffuse region of neutron skin or halo which can extend much further. The values of magic numbers of the nuclear shell model for neutron and protons are no longer sacrosanct. Indeed, the number of neutron-rich nuclei which can exist is far greater than anticipated: improvements in the treatment of the self-consistent nuclear problem, including more realistic estimates of correlations and clustering, predict a neutron drip line which seems to be constantly receding. AGATA will focus on all these aspects through studies of proton-rich nuclei at and beyond the proton drip line and the extension of the $N = Z$ line, neutron-rich nuclei towards the neutron drip line in medium heavy elements and the heaviest elements towards new super-heavy elements. The response of nuclei to angular momentum and temperature will be investigated by probing ultra-high spin states

produced in extremely cold reactions, metastable states at high spins and large deformations and multi-phonon giant resonances.

Nuclear scientists are looking forward to the deployment of these new tracking arrays, AGATA and GRETINA. In the case of AGATA the collaboration plans to commission and prove tracking in real time with a 15 detector (5 triple module) system at Legnaro National Laboratory in 2008. A design image of this sub-array is shown in Fig. 41. This will be followed by a physics campaign at Legnaro and subsequently at GANIL, France and the GSI laboratory in Germany. The array will be continually enhanced towards a 4π system that the collaboration will have realized in the middle of the next decade.

Many other fields took advantage of the improvements in Ge detector technology which were to a large extent driven by nuclear spectroscopy. Ge(Li) and HPGe detectors became standard tools for industrial, medical and environmental survey applications. The increased reliability of encapsulated Ge detectors made them ideal for application in space research, e.g. 2001 Mars Odyssey [113] and INTEGRAL [114]. The dramatic advance of position-sensitive Ge detectors and γ-ray tracking will have wide ranging applications in medical imaging, astrophysics, nuclear safeguards and radioactive waste monitoring as well as introducing a new plateau of detection capability for nuclear structure studies.

Acknowledgements

The development of germanium detectors and technology is the result of many experts working in the field for over 30 years. We would like to thank all those whom we have worked with over the years especially those in the current γ-ray tracking project AGATA. We express our thanks to Andreas Wiens and Herbert Hess for their help with the figures. The authors were supported by German Bundesministerium für Bildung und Technologie and the UK Science and Technology Facilities Council.

References

[1] H.R. Koch, et al., Nucl. Instrum. Methods 175 (1980) 401.
[2] E.M. Pell, J. Appl. Phys. 31 (1960) 291.
[3] D.V. Freck, J. Wakefield, Nature 193 (1960) 669.
[4] A.J. Tavendale, G.T. Ewan, Nucl. Instrum. Methods 25 (1963) 125.
[5] E. Eube, et al., Nucl. Instrum. Methods 130 (1981) 73.
[6] L. Cleemann, et al., Nuclear Phys. A386 (1982) 367.
[7] J. Simpson, P.A. Butler, L.P. Ekstrom, Nucl. Instrum. Methods 204 (1983) 463.
[8] R.N. Hall, T.J. Soltys, IEEE Trans. Nucl. Sci NS-18 (1971) 160.
[9] W.L. Hansen, Nucl. Instrum. Methods 94 (1971) 377.
[10] G.F. Knoll, Radiation Detection and Measurement, Wiley, New York, 2002.
[11] W.R. Leo, Techniques for Nuclear and Particle Physics Experiments, Springer, Heidelberg, 1994.
[12] A. Utsunomiya, et al., Nucl. Instrum. Methods A548 (2005) 455.
[13] D. Weisshaar, G. Gersch, T. Waasem, J. Eberth, University of Cologne (in press).
[14] R.H. Pehl, Phys. Today (1977) 50.
[15] R.H. Pehl, et al., IEEE Trans. Nucl. Sci NS-26 (1979) 321.
[16] T.W. Raudorf, et al., IEEE Trans. Nucl. Sci NS-31 (1984) 25314.
[17] H.G. Thomas, et al., Nucl. Instrum. Methods A332 (1993) 215 15. E.
[18] A. Pullia, G. Pascovici, et al., IEEE-NSSC3 (2004) 1411.
[19] A. Pullia, et al., IEEE Trans. Nucl. Sci. 53 (5) (2006) 2869.
[20] Hull, Charge collection physics in germanium detectors, Ph.D. Thesis, Indiana University.
[21] J. Eberth, Prog. Part. Nucl. Phys. 28 (1992) 495.
[22] D. Gutknecht, Nucl. Instrum. Methods A288 (1990) 13.

[23] G. Riepe, D. Protic, Nucl. Instrum. Methods 165 (1979) 31.
[24] E.L. Hull, et al., Nucl. Instrum. Methods A538 (2005) 651.
[25] E.L. Hull, Proc. 27th Seismic Research Review, LA-UR-05-6407, vol. 2, 2005, p. 795.
[26] American National Standards Institute, ANSI N42.14, 1991.
[27] L.L. Riedinger, et al., Phys. Rev. Lett. 44 (1980) 568.
[28] A. Johnson, et al., Phys. Lett. B34 (1971) 605.
[29] R. Beetz, et al., Nucl. Instrum. Methods 145 (1977) 353.
[30] H.J.M. Aarts, et al., Nucl. Instrum. Methods 177 (1980) 417.
[31] P.J. Twin, Workshop on Nuclear Structure at High Spin, Risø, Denmark, 1981, p. 135.
[32] P.J. Twin, Proc. Conf. on Instr. for Heavy Ion Nucl. Res., in: D. Schapira (Ed.) Nucl. Sci. Research Conf. Series, vol. 7, Harwood, p. 231.
[33] J.P. Sharpey-Schafer, J. Simpson, Prog. Particle Nucl. Phys. 21 (1988) 293.
[34] A.N. James, et al., Nucl. Instrum. Methods A267 (1988) 144.
[35] R.M. Diamond, F.S.A. Stephens, Proposal for a high resolution ball, LBNL (unpubl.).
[36] R.M. Diamond, Proc. Conf. on Instr. for Heavy Ion Nucl. Res., in: D. Schapira (ed.), Nucl. Sci. Research Conf. Series, vol. 7, Harwood, p. 259.
[37] R.M. Lieder, et al., Nucl. Instrum. Methods 220 (1984) 363.
[38] B. Herskind, et al., Nuclear Phys. A447 (1985) 395c.
[39] F.A. Beck, Proc. Conf. on Instr. for Heavy Ion Nucl. Res., in: D. Schapira (ed.), Nucl. Sci. Research Conf. Series, vol. 7, Harwood, p. 129.
[40] J.P. Martin, et al., Nucl. Instrum. Methods A257 (1987) 301.
[41] P.J. Twin, Phys. Rev. Lett. 57 (1986) 811.
[42] M.A. Bentley, et al., Phys. Rev. Lett. 59 (1987) 2141.
[43] C.W. Beausang, John Simpson, J. Phys. G: Nucl. Part. Phys. 22 (1996) 527.
[44] M.A. Deleplanque, R.M. Diamond (Eds.) Gammasphere Proposal, 1987. Preprint LBNL-5202.
[45] D.G. Sarantites, et al., Nucl. Instrum. Methods A381 (1996) 418.
[46] M.W. Simon, et al., Nucl. Instrum. Methods A452 (2000) 205.
[47] C.N. Davids, J.D. Larson, Nucl. Instr. Meth. B 40–41 (1989) 1224.
[48] D. Bazzacco, Proc. Workshop on Large γ-ray Detector Arrays, Chalk River, Canada, AECL-10613, p. 376.
[49] C. Rossi Alvarez, Nuclear Phys. News 3 (3) (1993).
[50] E. Farnea, et al., Nucl. Instrum. Methods Phys. Res. A400 (1997) 87.
[51] P. Spolaore, et al., Nucl. Instrum. Methods Phys. Res. A359 (1995) 500.
[52] C.W. Beausang, Nucl. Instrum. Methods A313 (1992) 37.
[53] F.A. Beck, Proc. Conf. on Physics from Large γ-ray Detector, Arrays, Berkeley, LBL 35687, CONF 940888, UCA13, 1994, p. 154.
[54] G. Duchêne, et al., Nucl. Instrum. Methods A432 (1999) 90.
[55] J. Eberth, et al., Nucl. Instrum. Methods A369 (1996) 135.
[56] M. Wilhelm, et al., Nucl. Instrum. Methods A381 (1996) 49.
[57] P. von Neumann-Cosel, Prog. Nucl. Part. Phys. 38 (1997) 213.
[58] P. von Brentano, et al., Phys. Rev. Lett. 76 (1996) 2029.
[59] R.D. Herzberg, et al., Phys. Lett. B390 (1997) 49 55.
[60] D. Pansegrau, et al., Phys. Lett. B484 (2000) 1.
[61] Z. Hu, et al., Phys. Rev. C62 (2000) 064315.
[62] J. Gerl, R.M. Lieder (Eds.) Upgrading to Euroball III, GSI Report, 1992.
[63] J. Simpson, Z. Phys. A 358 (1997) 139.
[64] O. Skeppstedt, et al., Nucl. Instrum. Methods A421 (1999) 531.
[65] A. Dewald, Proc. 98 Seminar on Nucl. Phys. with Radioactive Ion Beam and High Spin Nuclear Structure, Lanzhou, China, 1998, p. 31.
[66] W. Korten, and S. Lunardi (Eds.), Achievements with the Euroball spectrometer 1997–2003. www.lnl.infn.it/~annrep/other_reports/euroball/eb_index.htm.
[67] J. Eberth, et al., Prog. Part. Nucl. Phys. 38 (1997) 29.
[68] Gammasphere. www.physics.fsu.edu/GS10Yr/introduction.htm.
[69] W.F. Mueller, et al., Nucl. Instrum. Methods A466 (2001) 492 65.
[70] J. Simpson, et al., APH N.S. Heavy Ion Phys. 11 (2000) 159 66. F.
[71] F. Azaiez, Nuclear Phys. A654 (1999) 1003c.
[72] E. Clément, Phys. Rev. C 75 (2007) 054313.

[73] S.L. Shepherd, et al., Nucl. Instrum. Methods A434 (1999) 373.
[74] H.C. Scraggs, et al., Nucl. Instrum. Methods A543 (2005) 431.
[75] J. Eberth, et al., Prog. Nucl. Part. Phys. 46 (2001) 389.
[76] D. Habs, et al., Prog. Nucl. Part. Phys. 38 (1997) 111.
[77] I. Stefanescu, et al., Phys. Rev. Lett. 98 (2007) 122701.
[78] M.A. Deleplanque, et al., Nucl. Instrum. Methods A430 (1999) 292.
[79] I.Y. Lee, et al., Rep. Prog. Phys. 66 (2003) 1095.
[80] G.J. Schmid, et al., Nucl. Instrum. Methods A430 (1999) 69.
[81] Th. Kroell, et al., Nucl. Instrum. Methods A463 (2001) 227.
[82] K. Vetter, et al., Nucl. Instrum. Methods A452 (2000) 223.
[83] A. Lopez-Martens, et al., Nucl. Instrum. Methods A533 (2004) 454.
[84] K. Vetter, et al., Nucl. Instrum. Methods A463 (2000) 105.
[85] Th. Kroell, et al., Nucl. Instrum. Methods A565 (2006) 691.
[86] M. Descovich, et al., Nucl. Instrum. Methods A553 (2005) 535.
[87] J.J. Valiente Dobon, et al., Nucl. Instrum. Methods A505 (2003) 174.
[88] T. Steinhardt, et al.http://ireswww.in2p3.fr/ires/workshops/agata_week/talks/AGAW-IReS_Steinhardt.pdf (in press).
[89] I.Y. Lee, Nuclear Phys. A746 (1990) 641c.
[90] J. Simpson, Acta Physica Pononica B36 (2005) 1383.
[91] J. Gerl, Acta Physica Colonica B34 (2003) 2481.
[92] J. Simpson, R. Kruecken, Nucl. Phys. News Intl. 13 (2003) 15.
[93] E. Farnea, LNL Annual Report 2003, LNL-INFN(REP)-202/2004, p. 160.
[94] E. Farnea. http://agata.pd.infn.it/documents/simulations/comparison.html.
[95] L. Mihailescu, et al., Nucl. Instrum. Methods A447 (2000) 350.
[96] B. Bruyneel, et al., Nucl. Instrum. Methods A569 (2006) 764.
[97] B. Bruyneel, et al., Nucl. Instrum. Methods A569 (2006) 774.
[98] S. Ramo, Proc. IRE 27 (1939) 584.
[99] Zhong He, Nucl. Instrum. Methods A463 (2001) 250 91.
[100] http://mgs2005.in2p3.fr/Mgs.php.
[101] A. Oliariu, et al., IEEE Trans. Nucl. Sci. 53 (2006) 1028.
[102] F.C.L. Crespi, et al., Nucl. Instrum. Methods A570 (2007) 459.
[103] J. Van der Marel, et al., Nucl. Instrum. Methods A437 (1999) 538.
[104] J. Van der Marel, et al., Nucl. Instrum. Methods A447 (2002) 391.
[105] L. Milechina, B. Cederwall, Nucl. Instrum. Methods A508 (2003) 394.
[106] E. Farnea, LNL Annual Report 2003, Legnaro.
[107] I. Piqueras, et al., Nucl. Instrum. Methods A516 (2004) 122.
[108] C. Rossi Alvarez, AGATA Global Level Processing Meeting, May 2003. http://agata.pd.infn.it/documents/glp5152003/CarlosRossiAlvarez.pdf.
[109] L. Nelson, et al., Nucl. Instrum. Methods A573 (2007) 153.
[110] M. Dimmock. http://www.csnsm.in2p3.fr/groupes/strucnuc/AGATA/AGATAWEEK/tuesday-session1/characterization//dimmock.ppt.
[111] F. Recchia. http://www.csnsm.in2p3.fr/groupes/strucnuc/AGATA/AGATAWEEK/tuesday-session1/PSA//recchia.ppt103.
[112] I.Y. Lee, http://ns.ph.liv.ac.uk/AGATA/files/tuesday/GRETINA_status_Lee.pdf.
[113] R.S. Saunders, et al., Space Sci. Rev. 110 (1–2) (2004).
[114] C. Winkler, Exp. Astronomy 6 (1995) 71.
[115] D. Radford, et al., Eur. Phys. J. A 15 (2002) 171.